In: Turbulence: Theory, Types and Simulation
Editor: Russell J. Marcuso
ISBN: 978-1-61761-735-5

Chapter 3

UNSTEADY TURBULENCE IN A SHOCK: PHYSICAL AND NUMERICAL MODELLING IN TIDAL BORES AND HYDRAULIC JUMPS

Hubert Chanson[1]*, Pierre Lubin[2] and Stéphane Glockner[3]

[1]Professor in Civil Engineering. The University of Queensland, Brisbane QLD 4072, Australia

[2]Lecturer, Université de Bordeaux, TREFLE-ENSCBP UMR 8508 CNRS, 16 Avenue Pey-Berland, 33607 Pessac Cedex, France

[3]Research engineer, Université de Bordeaux, TREFLE-ENSCBP UMR 8508 CNRS, 16 Avenue Pey-Berland, 33607 Pessac Cedex, France

ABSTRACT

A turbulent flow is characterised by an unpredictable behaviour, a broad spectrum of length and time scales, and its strong mixing properties. Turbulent flows have a great mixing potential involving a wide range of vortical length scales. In steady flows, the turbulence measurements must be conducted at high frequency to resolve the small eddies and the viscous dissipation process. They must also be performed over a period significantly larger than the characteristic time of the largest vortical structures. In a highly unsteady flow, such as a shock, the experimental technique must be adapted, and this is detailed herein for positive surges, tidal bores and hydraulic jumps. A review of detailed turbulence measurements in tidal bores is conducted, and a number of laboratory experimental techniques are compared together with two- and three-dimensional large eddy simulation (LES) calculations. The experimental results demonstrate that the propagation of tidal bores induces some substantial turbulent mixing in natural estuaries. The passage of a tidal bore is associated with some large water depth fluctuations. Both the instantaneous and ensemble-averaged turbulent velocity data highlight some seminal features of the flow field in tidal bores. The instantaneous velocity measurements and the numerical data show a marked effect of the tidal bore front passage. The streamwise

* Corresponding author: Email: h. chanson@uq. edu. au - Url: http://www. uq. edu. au/~e2hchans/, Ph. : + 61 7 3365 3516 - Fax: +61 7 3365 4599

velocities are always characterised by a rapid flow deceleration at all vertical elevations, and large fluctuations of all velocity components are recorded beneath the surge and whelps. Both physical and numerical studies document the production of large coherent structures in tidal bores. The existence of such energetic turbulent events beneath and shortly after the tidal bore front implies the generation of vorticity during the bore propagation. Some experimental results show further that the variable interval time averaged (VITA) data based upon a single run present some non-negligible differences with the ensemble-averaged (EA) median results in terms of all velocity components. Both the EA and VITA methods showed some comparable long-term trends superposed to some rapid turbulent fluctuations, as well as close results in terms of the turbulent Reynolds stress components.

Keywords: Hydraulic jumps, Tidal bores, Turbulence, Unsteady flow, Shock, Physical modelling, Numerical modelling, Large eddy simulation LES, Ensemble average, Variable interval time average VITA.

1. Introduction

1.1. Presentation

Hydraulic jumps are commonly experienced in streams and rivers, as well as in industrial channels and manufacturing processes. A hydraulic jump is the rapid transition from a high-velocity open channel flow to a slower fluvial motion. It is a sharp discontinuity in terms of the water depth as well as the pressure and velocity fields (LIGHTHILL 1978) (Figure 1-1). The hydraulic jump is characterised by a highly turbulent flow with an air-water turbulent shear layer and a recirculation zone above. Some large scale coherent structures develop in the shear layer and interact with the free surface leading to strong splashing and droplet ejection above the two-phase flow region (Figure 1-1A). The impingement point is a source of both air entrainment and vorticity. Downstream some significant kinetic energy dissipation takes place.

A hydraulic jump in translation results from a sudden change in flow that increases the depth. Called a positive surge or bore, it is the quasi-steady flow analogy of the stationary hydraulic jump (HENDERSON 1966, LIGGETT 1994). The positive surges were studied by hydraulic engineers and applied mathematicians for a few centuries. Pertinent reviews comprised BENJAMIN and LIGHTHILL (1954), CUNGE (2003) and CHANSON (2009a,2010a). Although most studies of positive surges and bores considered horizontal channels, a range of practical applications encompasses some hydraulic jumps propagating upstream on downward sloping channels: e. g., step pool channels during a flash flood, rejection surges in power canals serving hydro-power stations during sudden decrease in power output, swash runup against rundown on a beach slope. When the bore propagates upstream against a supercritical flow on a steep slope, the surge will progressively decelerate and become a stationary hydraulic jump. A key feature of jumps, bores and surges is the intense turbulent mixing generated by the jump roller (HENDERSON 1966, PARKER 1996).

In a natural system, the formation and occurence of hydraulic jumps have some major impact on the channel bed and associated sediment transport (MACDONALD et al. 2009). For example, in a mobile bed flume, KENNEDY (1963) showed the impact of standing waves and CHANSON (2000) measured the boundary shear stress beneath undular hydraulic jumps. BELLAL et al. (2003) observed the bed deformation associated with the upstream propagation of a positive surge until its stabilisation and ultimately its disappearance in response to a change in bed topography. The formation of a hydraulic jump propagating upstream against a steep slope, its deceleration and vanishing were also associated with some cyclic behaviour (PARKER 1996, GRANT 1997, PARKER and IZUMI 2000, YOKOKAWA et al. 2009). Some pertinent studies included CARLING (1995) and MACDONALD et al. (2009) with the stationary hydraulic jumps, and CHEN et al. (1990), WOLANSKI et al. (2004) and KOCH and CHANSON (2008) in tidal bores. Other relevant studies encompassed the studies of bores generated by wave runup in the swash zone of the shoreline (KOBAYASHI 2001, BUTT et al. 2004, BARNES et al. 2009).

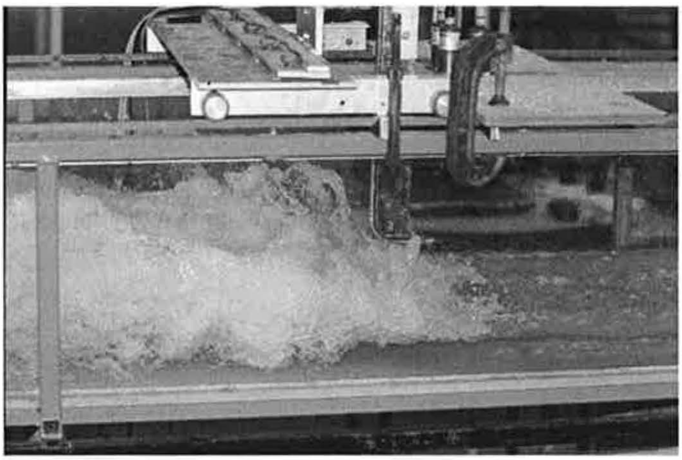

(A) Hydraulic jump in a rectangular laboratory channel - $Fr_1 = 4.32$, $Re=1.1\ 10^5$, shutter speed: 1/180s - Steady flow from right to left

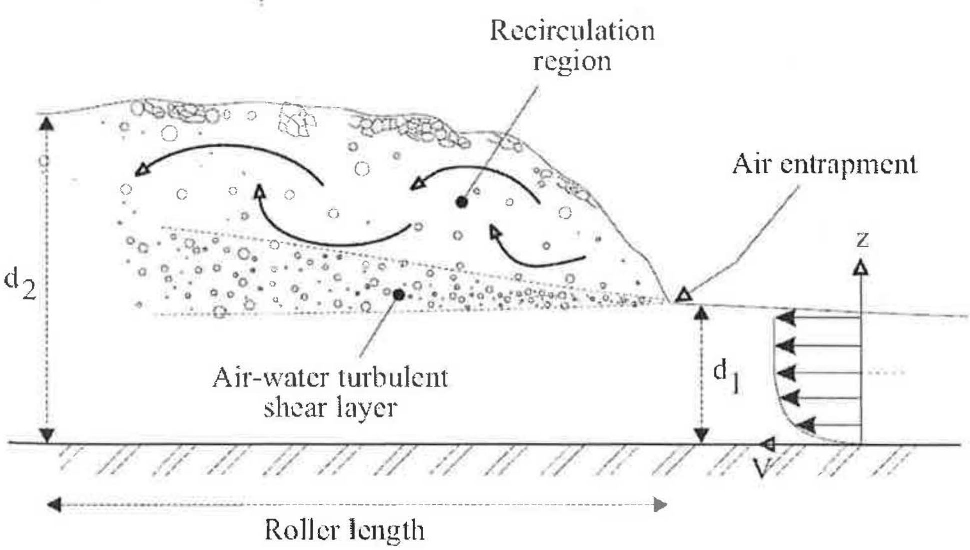

(B) Definition sketch

Figure 1-1. The stationary hydraulic jump.

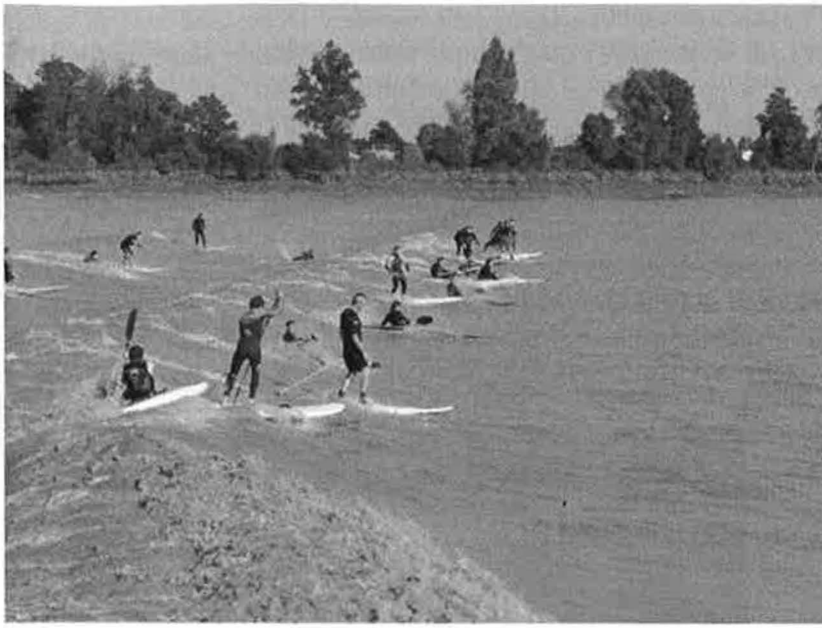

(A) Tidal bore of the Dordogne River on 29 Sept 2008 evening

(B) Tidal bore of the Qiantang River on 20 September 2008 (Courtesy of Pierre WEILL)

Figure 1-2. Photographs of tidal bores in natural estuaries - Bore propagation from left to right.

1.2. Tidal Bores

A tidal bore is an unsteady flow motion generated by the rapid water level rise at the river mouth during the early flood tide. With time, the leading edge of the tidal wave becomes steeper and steeper until it forms a wall of water: i. e., the tidal bore. After the formation of the bore, there is an abrupt rise in water depth at the bore front that is discontinuity in water depth and velocity field. Figure 1-2 shows the tidal bore of the Dordogne River in France and of the Qiantang River in China. Note the similarity in shape between the stationary hydraulic jump (Figure 1-1A) and the tidal bores (Figure 1-2) at a given instant. Once formed, the flow properties immediately before and after the tidal bore must satisfy the continuity and momentum principles (RAYLEIGH 1908, HENDERSON 1966, LIGGETT 1994). The integral form of the equations of conservation of mass and momentum gives a series of relationships between the flow properties in front of and behind the bore front. For a rectangular horizontal channel and neglecting bed friction, it yields:

$$\frac{d_2}{d_1} = \frac{1}{2} \times \left(\sqrt{1 + 8 \times Fr_1^{\ 2}} - 1 \right) \tag{1.1}$$

where d_1 is the initial water depth, d_2 is the downstream conjugate flow depth immediately after the bore passage, V_1 is the initial river flow velocity positive downstream, and U is the tidal bore celerity for an observed standing on the bank positive upstream (Figure 1-3). Fr_1 is the tidal bore Froude number defined as:

$$Fr_1 = \frac{V_1 + U}{\sqrt{g \times d_1}} \tag{1.2}$$

The Froude number Fr_1 of the tidal bore is defined in the system of co-ordinates in translation with the bore front. Fr_1 is always greater than unity. For $Fr_1 < 1$, the tidal wave cannot become a tidal bore.

A tidal bore is a hydrodynamic shock. The front is characterised by a sudden rise in free-surface elevation and a discontinuity of the pressure and velocity field. The tidal bore is a turbulent unsteady flow motion that is comparable to a shock.

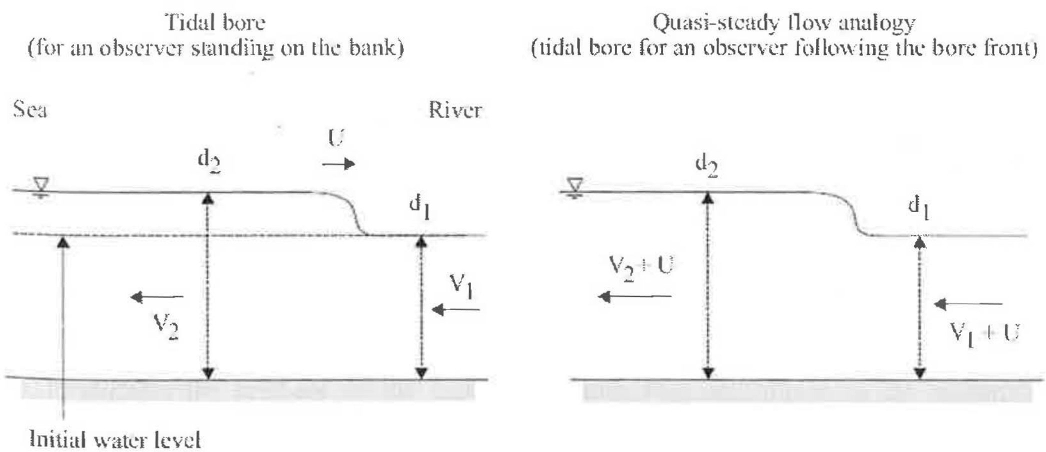

Figure 1-3. Definition sketch a tidal bore propagation and of the quasi-steady flow analogy applied to the bore front.

2. Turbulence Characterisation in Steady and Unsteady Flows

2.1. Presentation

In natural rivers and estuaries, the flow Reynolds number is within the range of 10^5 to 10^7 and more. The flow is turbulent: that is, it is characterised by an unpredictable behaviour, a broad spectrum of length and time scales, and some strong mixing properties. In his classical experiment, Osborne REYNOLDS (1842-1912) illustrated this key feature with the rapid mixing of dye of a turbulent flow (REYNOLDS 1883). In the turbulent flow, the fluid particles move in very irregular paths, causing an exchange of momentum from one portion of the fluid to another.

An experimental study of turbulence requires a long-duration data set recorded at high frequency. The fine spatial and temporal resolution is a prerequisite to gain insights into the characteristics of fine-scale turbulence. The turbulence measurements must be performed at high frequency to characterise the small eddies and the viscous dissipation process because the "*turbulence is a three-dimensional time-dependent motion in which vortex stretching causes velocity fluctuations to spread to all wavelengths*" (BRADSHAW 1971, p. 17). The measurements must further to be conducted for a sampling duration that is significantly longer than the characteristic time scale of the largest vortical structures to capture the pseudo-random nature of the flow and the deviations from Gaussian statistical properties. In a natural system, the turbulence is rarely homogeneous nor isotropic. Simply some detailed turbulence measurements are almost impossible unless some continuous sampling at high frequency is performed over a fairly long duration: i. e., at least a full tidal cycle to characterise the estuarine turbulence.

2.2. Turbulence Properties

The turbulent flows have a great mixing potential involving a wide range of eddy length scales (HINZE 1975). Although the turbulence is a "random" process, the small departures from a Gaussian probability distribution constitute some key features (BRADSHAW 1971). For example, the skewness and kurtosis give some information on the temporal distribution of the turbulent velocity fluctuation around its mean value. A non-zero skewness indicates some degree of temporal asymmetry of the turbulent fluctuation: e. g., acceleration versus deceleration, sweep versus ejection. The skewness retains some sign information and it can be used to extract basic information without ambiguity. An excess kurtosis larger than zero is associated with a peaky signal: e. g., produced by intermittent turbulent events.

In a steady turbulent flow, the instantaneous velocity is typically decomposed into a time-averaged component and a turbulent fluctuation. If the instantaneous velocity is V, $\overline{V}$ representes the time-averaged velocity and v is the instantaneous velocity fluctuation defined as:

$$v = V - \overline{V} \tag{2-1}$$

Similarly the pressure may be decomposed as:

$$p = \overline{P} - P \tag{2-2}$$

In Equations (2-1) and (2-2), the minuscule refers to the fluctuating parameter and the overbar corresponds to the time-averaged quantity. The time-average of a parameter V at a time t is defined as :

$$\overline{V} = \frac{1}{T} \times \int_{t-T/2}^{t+T/2} V \times dt' \tag{2-3}$$

In a steady flow, the integration period T must be large such that the time-average becomes independent of the limits, hence of the time t. Figure 2-1A presents a time-averaged steady flow data set. Both the instantaneous longitudinal velocity component and the time-averaged velocity are shown.

In a turbulent flow, the flux of the x-momentum in the y-direction induces an additional shear stress in the x-direction acting on the surface element normal to the y-direction. This additional stress is called the Reynolds stress or turbulent stress. It is denoted $\rho \times v_x \times v_y$, or more generally $\rho \times v_i \times v_j$ where i, j = x, y, z. The Reynolds stress $\rho \times v_i \times v_j$ characterises the additional shear stress on the faces $\delta x_i \delta x_j$ of an elementary control volume (δx, δy, δz), where x_i, x_j = x, y, z. The Reynolds stress tensor is a momentum transport effect resulting from turbulent motion induced by velocity fluctuations with its subsequent increase of momentum exchange and of mixing. The turbulent stress tensor components include both normal and tangential stresses, although there is no fundamental difference between normal stress and tangential stress (BRADSHAW 1971).

A Reynolds stress component may be expressed in a dimensionless form as a coefficient of correlation. The normalised cross-correlation coefficient is related to the Reynolds stress as:

$$R_{ij} = \frac{\rho \times \overline{v_i \times v_j}}{\rho \times \sqrt{\overline{v_i^2}} \times \sqrt{\overline{v_j^2}}} \tag{2-4}$$

where R_{ij} is the normalised cross-correlation coefficient function, i, j = x, y, z, and the time lag τ is zero ($R_{ij} = R_{ij}(\tau=0)$). The mean product $\overline{v_i \times v_j}$ is called the co-variance of v_i and v_j. Equation (2-4) is simply a dimensionless turbulent stress (CHANSON 2009b). A triple correlation characterises the transport of turbulent shear stress by velocity fluctuations (BRADSHAW 1976).

Physically, the gradient of the triple correlation R_{xxx} contributes to the streamwise diffusive flux of the streamwise kinetic energy $\overline{v_x^2}$. $\overline{v_x \times v_x \times v_y}$ represents the transport of $\overline{v_x \times v_y}$ in the x direction, while $\overline{v_x \times v_y \times v_y}$ describes the turbulent transport of $\overline{v_x \times v_y}$ in the y direction. More generally, R_{ijk} characterises in dimensionless form the transport of $\overline{v_j \times v_k}$ in the i direction, which is equal to the transport of $\overline{v_i \times v_j}$ in the k direction.

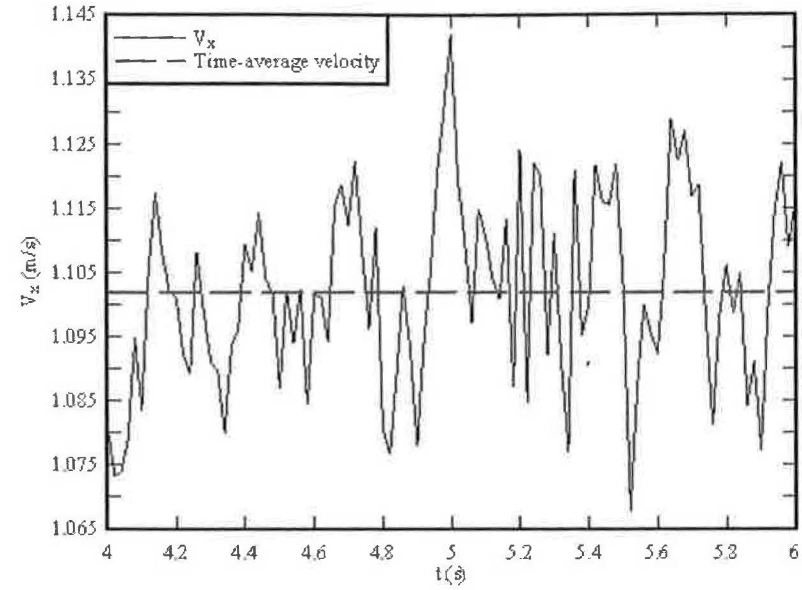

(A) Intantaneous longitudinal velocity component in a steady developing boundary layer flow: $z/d_1 = 0.72$, $z/\delta \approx 1$, $d_1 = 0.079$ m and $V_1 = 1.12$ m/s

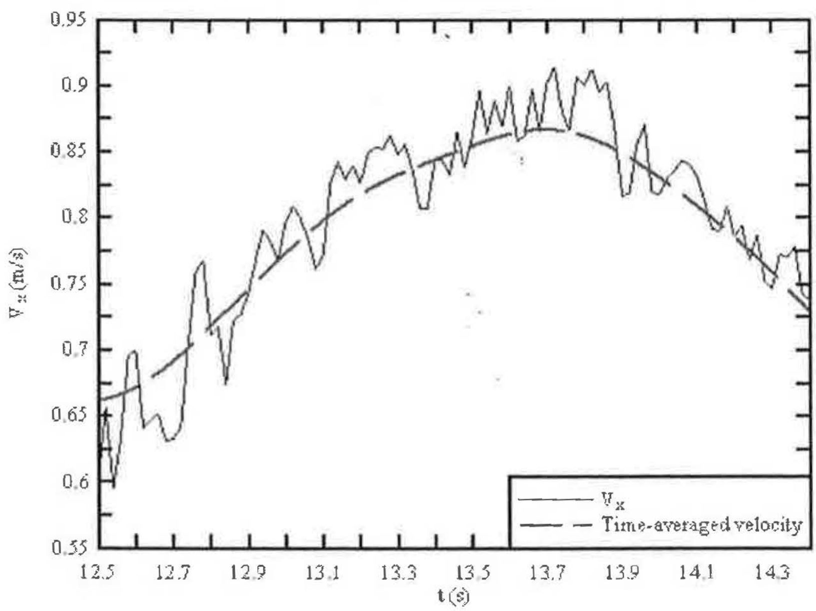

(B) Unsteady flow beneath an undular surge whelp ($Fr_1 = 1.4$) at $z/d_1 = 0.72$ on the channel centreline - VITA cutoff frequency: 1 Hz

Figure 2-1. Turbulence velocity fluctuations in steady and unsteady flows: longitudinal velocity component V_x in a turbulent open channel flow (after CHANSON 2009b) – Data collected with an acoustic Doppler velocimeter sampled at 50 Hz.

2.3. Unsteady Turbulence

When the flow is unsteady, a time average is not meaningful because the long-term trend and the short-term, turbulent fluctuations must be processed separately. The integration limits in Equation (2-3) must be large in comparison with the turbulent time scale but small compared to the time scale of the flow motion (BRADSHAW 1971, LIGGETT 1994, CHANSON 2009b). The turbulence in unsteady flows may be analysed using three different techniques: ensemble-averaging, phase-averaging and variable interval time averaging. The former is applicable to all unsteady flow conditions although its proper implementation is time-consuming. The phase averaging method may be used for simple periodic flows (e. g. regular wave motion); the characteristic flow period is divided into successive phases and the flow conditions are averaged for each phase. The technique is not relevant to a shock and will not be discussed any longer. The last technique, the variable interval time averaging, may be applied to gradually-varied flows.

If the unsteady turbulent flow is gradually-varied with some distinctive long-term and short-term fluctuation frequencies, $\overline{V}$ is a low-pass filtered component, or variable-interval time average VITA (PIQUET 1999). A cutoff frequency F_{cutoff} is required such that the characteristic time $1/F_{cutoff}$ is greater than the characteristic period of turbulent fluctuations, and small with respect to the characteristic period for the time-evolution of the mean properties (PIQUET 1999, GARCIA and GARCIA 2006, KOCH and CHANSON 2008). The instantaneous fluctuation v becomes the high-pass filtered component of the measured quantity.

In a transient, highly unsteady flow, the quantities of the mean motion are determined by ensemble-averaging. The same experiment is repeated N times and the ensemble average is defined as:

$$\overline{V}(x,y,z,t) = \frac{1}{N} \times \sum_{i=1}^{N} V_i(x,y,z,t) \tag{2-5}$$

The turbulent velocity fluctuation v becomes the deviation of the instantaneous velocity V from the ensemble average $\overline{V}$ (BRADSHAW 1971).

Figure 2-1B presents some unsteady flow data. The data set shown in Figure 2-1B corresponds to some turbulent velocity measurements beneath an undular positive surge, and $\overline{V}$ is the VITA. A comparison between Figures 2-1A and 2-1B illustrates the differences between steady and unsteady gradually-varied flows.

3. Physical Measurements in Tidal Bores

3.1. Presentation

The analytical and numerical studies of turbulent mixing in tidal bores are difficult considering the large number of relevant equations and the flow unsteadiness. Experimental investigations are not easy but some advances in metrology (e. g. particle image velocimetry

(PIV), acoustic Doppler velocimetry (ADV)) provide new means for successful turbulence measurements (HORNUNG et al. 1995, KOCH and CHANSON 2008,2009).

The laboratory studies are performed with geometrically similar models for which the geometric scaling ratio L_r is defined as the ratio of prototype to model dimensions. The model studies of tidal bores require the selection of an adequate similitude. In any study of turbulent flows, the relevant parameters needed for any dimensional analysis include the fluid properties and physical constants, the channel geometry and inflow conditions, and possibly the entrained air bubble characteristics. For a tidal bore propagating in a horizontal, rectangular channel, a simplified dimensional analysis yields:

$$V_x, V_y, V_z = F_1(x, y, z, t, U, d_1, V_1, \delta, B, g, \rho, \mu, \sigma ...) \tag{3-1}$$

where V_x, V_y, V_z are respectively the longitudinal, transverse and vertical velocity components at a location (x, y, z), x is the coordinate in the flow direction, y is the horizontal transverse coordinate measure d from the channel centreline, z is the vertical coordinate measured from channel bed, t is the time, U is the surge celerity, d_1 is the initial depth, V_1 is the initial flow velocity, δ is the boundary layer thickness at x, B is the channel width, g is the gravity acceleration, ρ and μ are the water density and dynamic viscosity respectively, and σ is the surface tension between air and water.

In Equation (3-1), the turbulent flow properties (left handside terms) at a position (x, y , z) and at a time t are expressed as functions of the tidal bore properties, initial flow properties, channel geometry and fluid properties. In addition, the biochemical properties of the water solution may be considered especially in natural estuarine systems. Note that compressibility of the bubbles might be an important issue in breaking bores.

For a tidal bore, the relevant characteristic length scale is the initial flow depth d_1 and the relevant Froude number is the tidal bore Froude number defined in Equation (1-2). Equation (3-1) may be rewritten in dimensionless terms:

$$\frac{V_x}{V_1}, \frac{V_y}{V_1}, \frac{V_z}{V_1} = F_2\left(\frac{x}{d_1}, \frac{y}{d_1}, \frac{z}{d_1}, t \times \sqrt{\frac{g}{d_1}}, \frac{V_1 + U}{\sqrt{g \times d_1}}, \rho \times \frac{(V_1 + U) \times d_1}{\mu}, \frac{\delta}{d_1}, \frac{B}{d_1}, \frac{g \times \mu^4}{\rho \times \sigma^3}, ...\right) \tag{3-2}$$

In Equation (3-2) right handside, the fifth and sixth terms are the tidal bore Froude and Reynolds numbers respectively, and the ninth term is the Morton number which is a function only of fluid properties and gravity constant. For the same fluids (air and water) in both model and prototype, the Morton number becomes a constant.

Dynamic similarity and scale effects

In a geometrically similar model, a true dynamic similarity is achieved only if each dimensionless parameters (or Π-terms) has the same value in both model and prototype. Scale effects may exist when one or more Π-terms have different values between model and prototype.

In free-surface flows including hydraulic jumps and tidal bores, the gravity effects are important and a Froude similitude is commonly used (HENDERSON 1966, CHANSON 1999,2004). That is, the model and prototype Froude numbers must be equal. But the entrapment of air bubbles in a breaking bore roller is dominated by surface tension effects. Similarly, the turbulent mixing processes are dominated by viscous forces implying the needs for a Reynolds similitude. Figures 1-2 and 3-1 illustrate indeed the intense turbulence of a tidal bore in a natural system.

For geometrically-similar models, it is impossible to satisfy simultaneously all the similarities. Basically the dynamic similarity of turbulent tidal bores is nearly impossible because of too many relevant parameters (Eq. (3-2)). In practice, the physical studies are based upon a Froude similitude, but no systematic study was conducted to date to assess the scale effects affecting the turbulent mixing in tidal bore flows (Figure 3-1).

It is worth noting that the above analysis (Eq. (3-2)) does not account for the physio-chemical properties of the water, the air entrainment in the bore roller nor the characteristics of the instrumentation. The size of the probe sensor, the sampling rate and possibly other probe characteristics do affect the minimum length and time scales detectable by the instrumentation. For example, in the particular case of intrusive probe (e. g. ADV probes), the sampling volume may be larger than the smallest vortical structures.

3.2. Physical Experiments

Unsteady turbulent measurements in tidal bores are limited, but for a few laboratories studies under well-defined, controlled flow conditions (Table 3-1, Figure 3-2). Table 3-1 lists the experimental flow conditions of these studies and Figure 3-2 presents a schematic of the two experimental, rectangular channels. The first study considered two reservoirs initially at rest, with different initial water depths and separated by a vertical sluice gate. The rapid removal of the gate formed a dam break wave led by a bore that propagated over the water initially at rest (Figure 3-2A). The turbulent velocity measurements were performed with particle image velocimetry (PIV) sampled at 15 Hz. The second series of studies was characterised by an initially steady, subcritical flow motion and the tidal bore was generated by the rapid closure of a tainter gate at the channel downstream end (Figure 3-2B). The turbulence measurements were performed using acoustic Doppler velocimetry (ADV) with a sampling rate of 50 to 200 Hz.

Figure 3-1. Turbulent tidal bore of the Qiantang River (China) on 23 July 2009 (Courtesy of Jean-Pierre GIRARDOT) – Propagation from left to right.

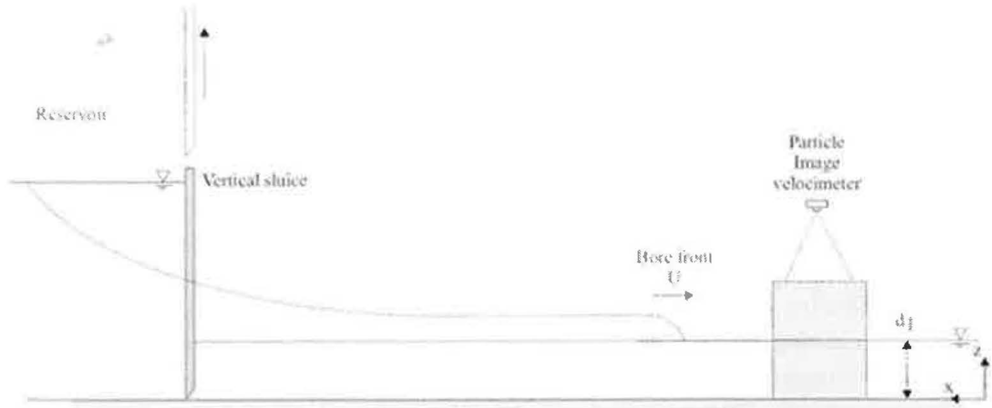

(A) Physical modelling at Caltech (HORNUNG et al. 1995)

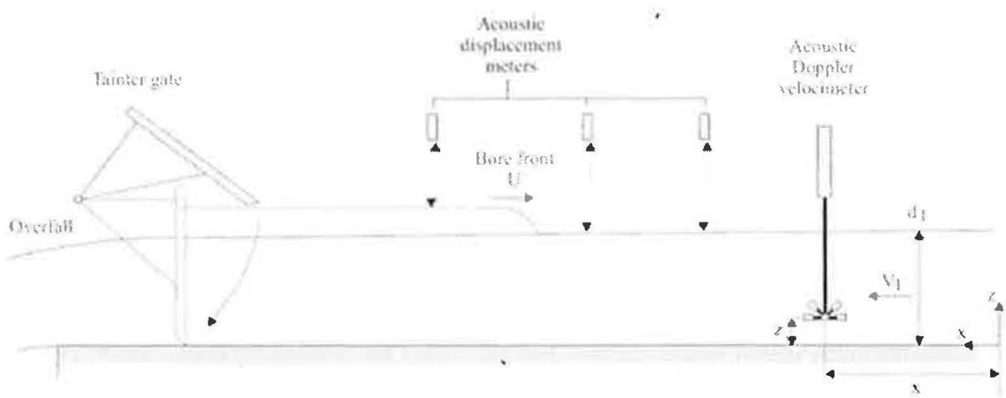

(B) Physical modelling at the University of Queensland (KOCH and CHANSON 2009, CHANSON 2010b,2009c, DOCHERTY and CHANSON 2010)

Figure 3-2. Turbulence measurements in laboratory facilities: experimental configurations.

All studies were conducted based upon a Froude similitude, but with different initial conditions. In the first study, the flow was initiallly at rest. In the second facility, the initial flow was a turbulent flow motion, and the new flow conditions after the bore passage were characterised by a slower downstream motion. Neither arrangements reproduced the tidal bore motion in a natural estuary, where the initial flow velocity V_1 is non-zero, positive downstream and the flood flow velocity V_2 behind the bore is typically positive upstream. Further all the experiments were conducted with freshwater and the Reynolds number in the laboratory channels was about one to two orders of magnitude smaller than in most natural estuarine systems.

Turbulent velocity calculations

With a PIV technique, the main outputs are the instantaneous velocity and vorticity fields, as well as their time-variations. With an Eulerian measurement technique (e. g. ADV, LDA), the time variations of the velocity components are recorded prior to, during and shortly after the tidal bore passage. Herein V_x is the longitudinal velocity positive downstream, V_y is the horizontal transverse velocity and V_z is the vertical velocity positive upwards (Figure 3-

2). The turbulent velocity fluctuations may be derived using either the ensemble-average method (EA) or the variable interval time average technique (VITA).

DOCHERTY and CHANSON (2010) tested both the ensemble-average and VITA techniques with the repetition of 20 identical experiments. For the VITA method, an upper limit of the filtered signal was the Nyquist frequency while a lower limit was a period of about 0. 9 s that corresponded to the period of the residual undulations. The final cut-off frequency was selected based upon a sensitivity analysis that yielded an optimum threshold of F_{cutoff} and the filtering was applied to all velocity components. Both KOCH and CHANSON (2008) and DOCHERTY and CHANSON (2010) selected a cutoff period $1/F_{cutoff}$ that was about half the secondary wave period.

3.3. Basic Observations

The physical experiments (Table 3-1) indicated systematically some seminal flow features. For a tidal Froude number Fr_1 between unity and 1. 5 to 1. 8, the tidal bore was undular: that is, the wave front was followed by a train of secondary, quasi-periodic waves called undulations or whelps (Figure 3-3A). For larger Froude numbers, a breaking bore was observed (Figure 3-3B). The basic flow pattern observations were consistent with the earlier free-surface measurements of FAVRE (1935), BENET and CUNGE (1971) and TRESKE (1994). Two examples of undular and breaking bores are shown in Figure 3-3 and the details of the experimental conditions are reported in the figure captions.

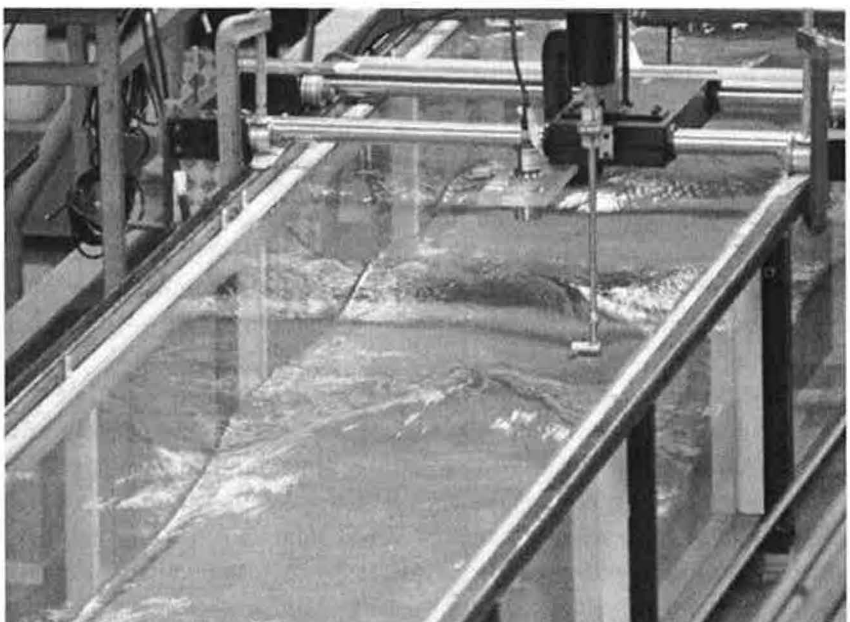

(A)

Undular bore: $Fr_1 = 1.4$, $\rho\times(V_1+U)\times d_1/\mu = 0.97\times10^5$, $d_1 = 0.079$ m, $V_1 = 1.0$ m/s, $B = 0.5$ m

Figure 3-3. Continued.

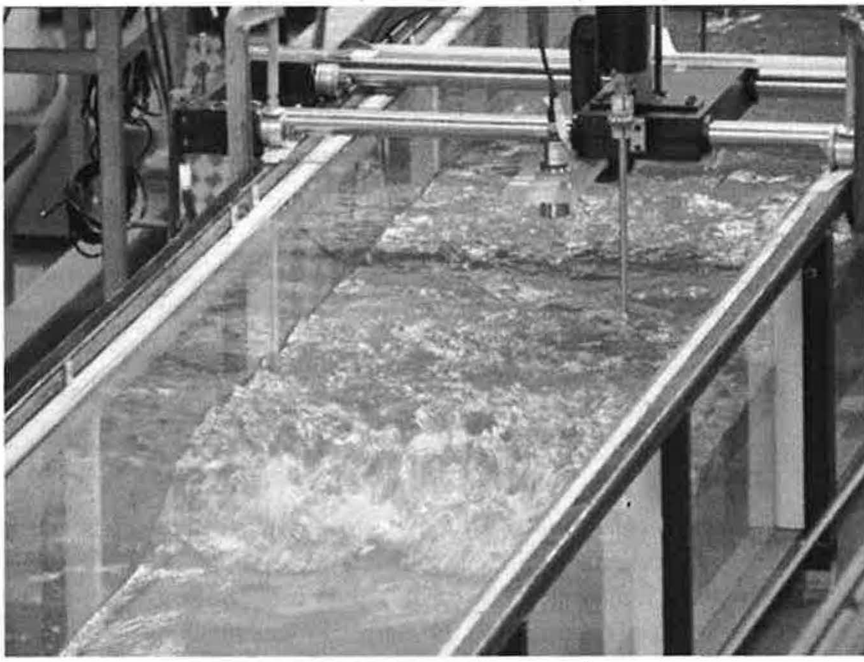

(B) Breaking bore: $Fr_1 = 1.8$, $\rho\times(V_1+U)\times d_1/\mu = 1.2\times10^5$, $d_1 = 0.079$ m, $V_1 = 1.0$ m/s, B = 0.5 m

Figure 3-3. Photographs of undular and breaking tidal bore experiments - Bore propagation from top right to bottom left.

The turbulent velocity measurements showed that the arrival of the tidal bore and the sudden increase in water depth yielded a rapid change in longitudinal velocity to satisfy the conservation of mass. In a natural river, a flow reversal ($V_x < 0$) is often observed. The longitudinal velocities were characterised by a rapid flow deceleration at all vertical elevations, while some large fluctuations of longitudinal, transverse and vertical velocity components were observed beneath the tidal bore. The tidal bore was basically a shock characterised by a sudden change in the velocity field (LIGHTHILL 1978). The shock was followed by a highly turbulent flow motion with significant fluctuations of all velocity components. Typical Eulerian measurements are presented in Figure 3-4 for an undular tidal bore and a breaking bore.

In an undular tidal bore, the longitudinal velocity V_x oscillated with time with the same period as, but out of phase with, the free-surface undulations immediately after the front (KOCH and CHANSON 2008, CHANSON 2009c). When the undular bore front passed the sampling point, a relatively gentle longitudinal flow deceleration was observed at all vertical elevations. The longitudinal velocity component was minimum beneath the first wave crest and it oscillated afterwards with the same period as the surface undulations and out of phase (Figure 3-4A). The vertical velocity data presented a similar oscillating pattern beneath the free-surface undulations with the same periodicity, and out of phase. The data trends were consistent with the irrotational flow theory (ROUSE 1938, LIGGETT 1994, CHANSON 2009b).

Table 3-1. Physical studies of and turbulence measurements in tidal bores

Reference	Q	B	S_o	d_1	Fr_1	Bed	Instrumentation
	(m^3/s)	(m)		(m)		roughness	
(1)	(2)	(3)	(4)	(5)	(6)	(7)	(8)
HORNUNG et al. (1995)	0	--	0	--	1. 5 to 6	Smooth bed	PIV, sampling: 15 Hz, 500×650 pixels, 1 pixel = 0. 2×0. 2 mm^2.
KOCH & CHANSON (2009)	0. 040	0. 50	0	0. 079	1. 31 to 1. 93	Smooth PVC	MicroADV (16 MHz), sampling: 50 Hz, sampling volume: 4. 2×4. 2×6. 2 mm^3.
CHANSON (2010b)	0. 058	0. 50	0	0. 137	1. 17 to 1. 49	Smooth PVC	Vectrino+ ADV (10 MHz), sampling: 200 Hz, sampling volume: 6×6×1. 5 mm^3.
				0. 142 ($^+$)	1. 13 to 1. 47	Plastic screens	k_s = 6. 6 mm
CHANSON (2010c)	0. 058	0. 50	0. 0145	0. 070	2. 0	Smooth PVC	Vectrino+ ADV (10 MHz), sampling: 200 Hz, sampling volume: 6×6×1. 5 mm^3.
CHANSON (2009c)	0. 019	0. 50	0	0. 115 to 0. 20	1. 08 to 1. 2	Smooth PVC	Vectrino+ ADV (10 MHz), sampling: 200 Hz, sampling volume: 6×6×1. 5 mm^3.
DOCHERTY & CHANSON (2010)	0. 050	0. 50	0	0. 118	1. 08 to 1. 59	Smooth PVC	Vectrino+ ADV (10 MHz), sampling: 200 Hz, sampling volume: 6×6×1. 5 mm^3.
			0. 002	0. 125 ($^+$)	1. 01 to 1. 52	Fixed gravel bed	k_s = 3. 4 mm

Notes: B: channel width; d_1: initial water depth; Fr_1: tidal bore Froude number; k_s: equivalent sand roughness height; Q: initial flow rate; S_o: bed slope; ($^+$): measured above the roughness; All experiments were performed with tap water.

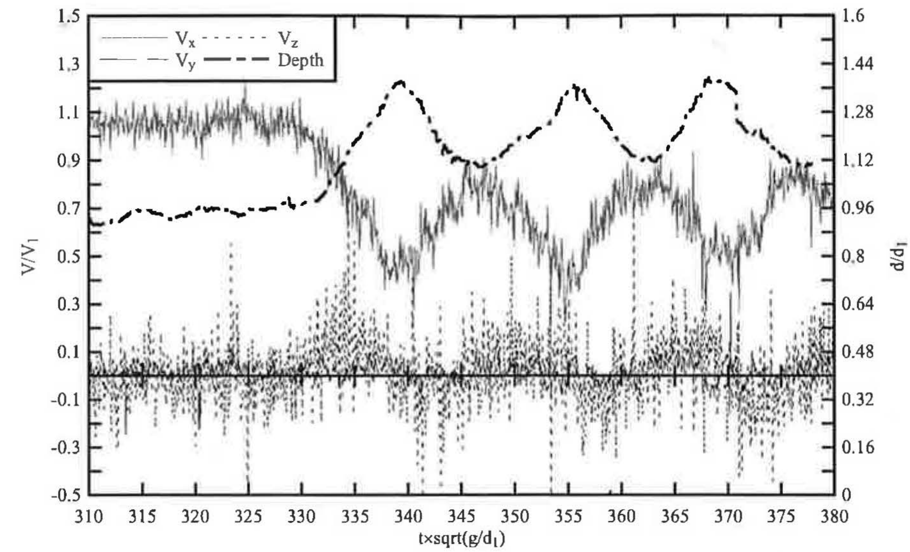

(A) Undular bore: $Fr_1 = 1.17$, $\rho\times(V_1+U)\times d_1/\mu = 1.9\times10^5$

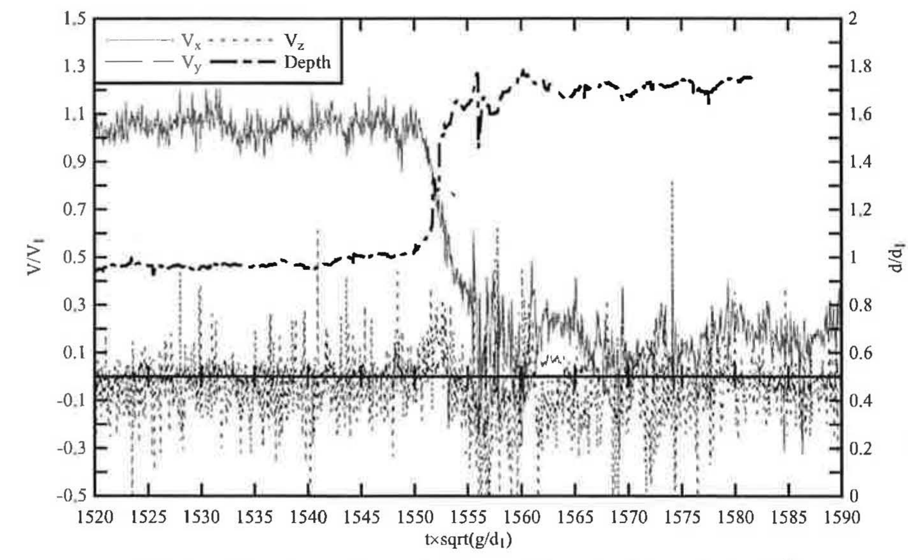

(B) Breaking bore: $Fr_1 = 1.50$, $\rho\times(V_1+U)\times d_1/\mu = 2.4\times10^5$

Figure 3-4. Time variations of the water depth and longitudinal, transverse and vertical velocity components in undular and breaking tidal bores – $d_1 = 0.138$ m, $V_1 = 0.83$ m/s, $z/d_1 = 0.76$, $B = 0.5$ m, smooth PVC bed (Data: CHANSON 2010b).

The breaking tidal bore data showed a sharp front with a marked roller and some bubble entrainment. The free-surface was typically curved upwards immediately prior to the roller toe. The gentle rise of the free-surface could be linked with a gradual decrease of the longitudinal velocity component at all vertical elevations as shown by HORNUNG et al. (1995), KOCH and CHANSON (2009) and DOCHERTY and CHANSON (2010). The roller passage corresponded to a sudden decrease of the longitudinal velocity component. The flow deceleration was notably sharper than that for an undular bore at all vertical elevations (Figure 3-4B). In the breaking tidal bore, the velocity data showed a further distinctive feature. Close to the bed (z/d_1 < 0. 2 to 0. 5), the instantaneous dimensionless longitudinal velocity $(V_x-V_2)/(V_1-V_2)$ could become negative highlighting a relatively rapid transient associated with some unsteady flow separation (KOCH and CHANSON 2009, DOCHERTY and CHANSON 2010).

In addition, the velocity measurements highlighted some energetic turbulent events beneath and behind the tidal bore front. These were best seen by some sudden and rapid fluctuations of the transverse and vertical velocity components (KOCH and CHANSON 2009, CHANSON 2009c,2010a), while some recent numerical modelling highlighted the production of large turbulent eddies beneath the bore front and their upstream advection behind the bore (LUBIN et al. 2010b). These vortical structures remained next to the bed as the bore propagated upstream while the presence of these persisting, coherent structures indicated that a great amount of sediment matters could be placed in suspension and advected upstream in a natural estuary. Such vigorous and energetic turbulent events were some form of macro-turbulence that was likely induced by some secondary motion. In the Daly River (Australia), a period of very strong turbulence was observed about twenty minutes after the bore passage lasting for about three minutes: "*about 20 min after the passage of the undular bore, a 3-min-duration patch of macro-turbulence was observed. [...] This unsteady motion was sufficiently energetic to topple moorings that had survived much higher, quasi-steady currents of 1. 8 m/s (Wolanski et al., 2001)*" (WOLANSKI et al. 2004) (Figure 3.5).

The observations of large transverse and vertical velocity fluctuations behind the tidal bore implied the existence of transient secondary currents behind the bore front that were associated with some unsteady transverse shear pattern (Figure 3-6). The vorticity "clouds" were a characteristic feature of the tidal bores that were linked with some secondary current motion and are enhanced in the natural, non-prismatic channels.

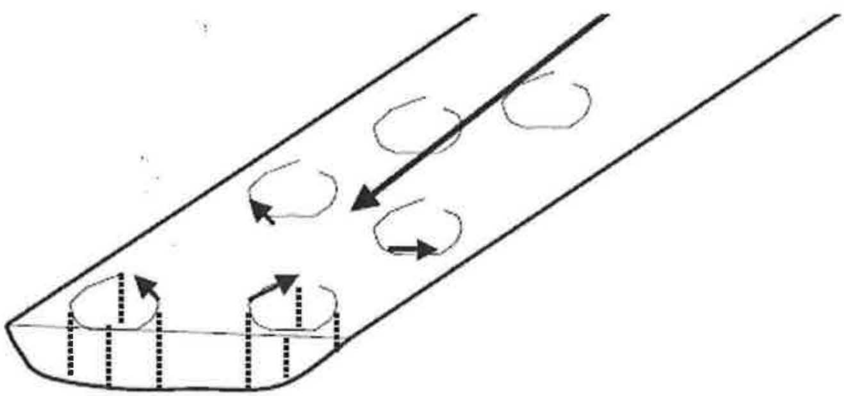

Figure 3.5. Surface macro-scale turbulence advected upstream behind the tidal bore of the Daly River and observed 20 minutes after the bore passage (after WOLANSKI et al. 2004).

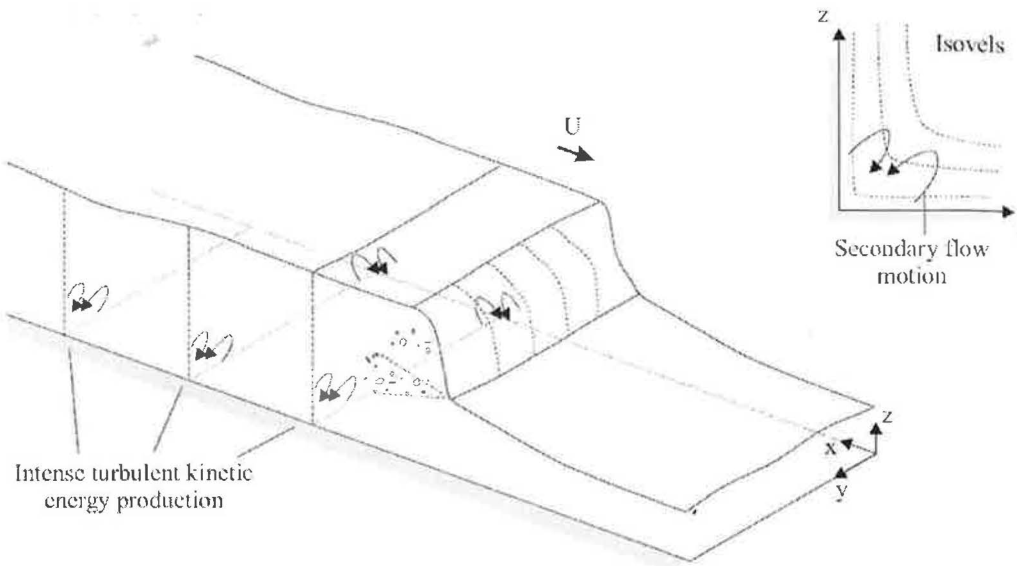

Figure 3.6. Secondary currents in a tidal bore propagating in a rectangular channel - Inset: secondary flow motion in the corner.

Discussion

Further field studies highlighted some unusual mixing processes. Some transient fronts were observed behind the tidal bore in Baie du Mont Saint Michel (France) (CHANSON 2010a). These induced further secondary currents and vertical circulation. The front arrived typically a couple of minutes after the bore front and lasted several minutes. The presence of a transient front influenced the horizontal dispersion and residual circulation, and it had some significant impacts on the local chemical and biological processes.

On the other hand, in the Bay of Fundy (Canada), some inverted vertical stratification was observed whereas the surface waters had a higher salinity than the bottom waters immediately after the tidal bore passage (TULL 1997). It was suggested that the brackish waters overrode the fresh waters during the tidal bore propagation. Such an unstable water column stratification was followed rapidly by a rapid homogenisation of the vertical salinity associated with a rapid vertical mixing.

4. Numerical Modelling of Bores and Surges

4.1. Presentation

Few numerical studies of bores and surges were conducted to date. Recently the depth-averaged shallow water equations were used to simulate the tidal bore in Qiantang River (China) (MADSEN et al. 2005). However only numerical tools based upon the Navier-Stokes equations can give access to the complicated turbulent flow motion. A recent numerical study (FURUYAMA and CHANSON, 2008) was compared to laboratory experiments (KOCH and CHANSON 2009). Some interesting features were observed, but the results lacked a fine mesh grid resolution and accurate numerical schemes. More recently, LUBIN et al. (2010a,2010b) presented some two dimensional numerical results, based upon the solution of the Navier-Stokes equations in air and water coupled with a subgrid scale turbulence model (Large Eddy Simulation - LES). The numerical tool is well suited to deal with strong interface deformations occurring during wave breaking, for example, and with turbulence modelling in the presence of a free surface in a more general way. A summary is presented herein, and its extension to three-dimensional modelling is discussed.

4.2. Numerical Modelling

An incompressible multiphase phase flow between non-miscible fluids can be described by the Navier-Stokes equations associated to an advection equation of a phase function C used to locate the different media (C = 0 in the air and C = 1 in the water). In practice, C = 0. 5 is used to locate the interface. The governing equations for the large eddy simulation (LES) of an incompressible fluid flow are classically derived by applying a convolution filter to the unsteady Navier-Stokes equations. The resulting set of equations is:

$$\nabla.V = 0 \tag{4-1}$$

$$\rho \times \left(\frac{\partial V}{\partial t} + (V.\nabla)V \right) = \rho \times g - \nabla P + \nabla.((\mu + \mu_T) \times (\nabla V + \nabla^T V)) \tag{4-2}$$

$$\frac{\partial C}{\partial t} + (V.\nabla)C = 0 \tag{4-3}$$

$$\rho = C \times \rho_a + (1 - C) \times \rho_w \tag{4-4A}$$

$$\mu = C \times \mu_a + (1 - C) \times \mu_w \tag{4-4B}$$

where V is the velocity, P is the pressure, μ_T is the turbulent viscosity, t is the time, ρ_a and ρ_w are respectively the air and water densities, and μ_a and μ_a are the dynamic viscosities of air and water respectively.

The large scale turbulence is described by solving the flow equations (Eqs. (4-1) & (4-2)), while the small scale turbulence which is not resolved by the flow model is taken into account through a sub-grid scale model. To represent the dissipative effect of the small turbulent structures, the turbulent viscosity μ_T is calculated with the Mixed Scale model (SAGAUT 1998).

The time discretisation is implicit. The velocity/pressure coupling is solved with a pressure correction method, which consists in splitting the Navier-Stokes system into two stages: a velocity prediction and a pressure correction (GODA 1978). The equations are discretised on a staggered Cartesian grid thanks to the finite volume method. The space derivatives of the inertial term are discretised by a hybrid Upwind-Centered scheme and the viscous term is approximated by a second order centered scheme (PATANKAR 1990). The message passing interface (MPI) library is used to parallelise the code. The mesh is partitioned into equal size sub-domains to ensure load balancing. Communications between processors are also minimized. The high performance preconditionners (HYPRE) parallel solver and preconditioner library is used to solve the linear systems (FALGOUT et al. 2006). The prediction and correction steps are solved respectively using a bi-conjugate gradient stable algorithm (BICGStab) solver, associated with a point Jacobi pre-conditioner, and a generalised minimal residual method (GMRES) solver, associated with a multi-grid pre-conditioner. Further details are presented by LUBIN et al. (2010a, 2010b). A dual grid, or underlying grid, is used to gain an improved accuracy for the interface description, the mesh grid size being divided by two in each direction for the interface tracking (RUDMAN 1998). This technique also allows to avoid the interpolations of the physical characteristics on the staggered grids, since the phase function is defined on each point where the viscosities and densities are required. The interface tracking is achieved by a Volume of Fluid method (VOF): i. e. a Lax-Wendroff TVD scheme (Total Variation Diminishing) which is able to handle interface reconnections without interface reconstruction (LEVEQUE 1992).

Numerical validation

The experimental configuration is the generation of a weak tidal bore by a rapid partial gate closure at the downstream end of the numerical domain and its upstream propagation against the initially steady flow, as presented in the previous sections. The numerical configuration consists in an initial rectangular steady flow motion (from the right side of the numerical domain to the left side) with an initial steady velocity (V_o = 1. 021 m/s) impacting a wall boundary located at the left side of the numerical domain. When the initial rectangle of water hits the wall, the water runs-up the wall and splashes down. A breaking bore is generated and propagates upstream, towards the right side of the numerical domain (LUBIN et al. 2010a, 2010b).

LUBIN et al. (2010a, 2010b) used a 2D numerical domain, 10 m long and 1 m high (Figure 4-1). The initial water depth was d_o = 0. 0785 m. A no-slip condition was imposed at the lower boundary and an open boundary condition was used at the top of the numerical domain. At the left side of the numerical domain, an outlet velocity condition (V_{out} = 1. 76 m/s) was fixed to allow the water flow below a vertical gate as observed in the physical facility, the outlet height being h_{out} = 0. 02 m. The inlet velocity ($V_{in} = V_1$ = 1. 021 m/s) was fixed at the right side of the numerical domain as well as the inlet height $h_{in} = d_1$ = 0. 0785 m. The time step was chosen to ensure a Courant-Friedrichs-Levy number less equal to 0. 1. The calculation was conducted with the densities and viscosities of air and water (ρ_a = 1. 1768 kg/m^3 and ρ_w = 1000 kg/m^3, $\mu_a = 1.85 \times 10^{-5}$ Pa. s and $\mu_w = 1\times10^{-3}$ Pa. s). A hydrostatic pressure field was initialised in the rectangle of water. The numerical domain, discretised into 2000 × 1000 regular Cartesian cells, was partitioned into 256 sub-domains (one processor per sub-domain). The tidal bore Froude number was Fr_1 = 1. 77. Some large structures were observed and described: a main recirculation structure observed beneath the bore front and propagating upstream (towards the right side of the numerical domain), and some macro-turbulent structures separating for the previous one and propagating downstream (towards the left side of the numerical domain).

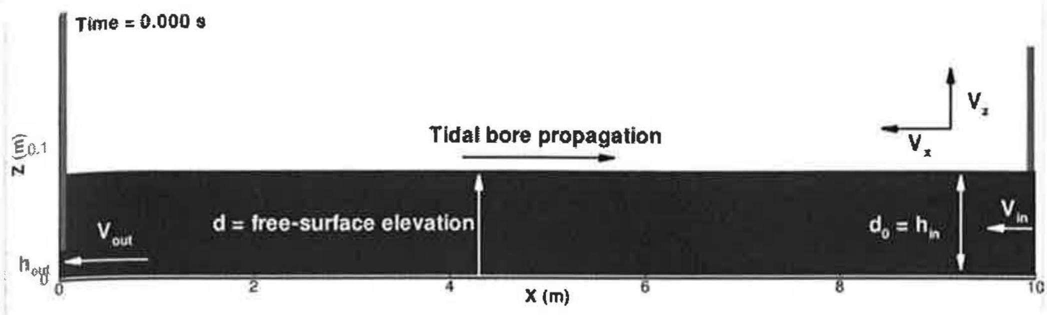

Figure 4-1. Sketch of the initial conditions for the tidal bore generation, immediately after the gate closure corresponding to the wall boundary condition set at the left side of the numerical domain.

4.3. Two-Dimensional Modelling

The initial large free-surface deformations were shown to be in agreement with the experimental photographs and movies. The celerity of the bore front was approximately 0. 5 m/s, that is close to the experimental value of 0. 54 m/s recorded at x = 5 m (KOCH and CHANSON 2009). The velocity field illustrated the strong agitation generated in the air domain by the bore generation. The bore front passage was shown to be associated with a rapid flow deceleration, coupled with a sudden increase in water depth. The numerical data were qualitatively in agreement with the experimental data. Some flow reversal (negative values of streamwise velocity) was observed next to the bed. This pattern was associated with some transient flow separation and recirculation. The largest vertical velocity magnitudes were observed next to the bed when the bore front was passing. Larger vertical velocity variations were recorded in the upper part of the water column, associated with air entrainment, splashes, free-surface fluctuations and vortical structures present in the roller.

Some large recirculation structures were observed beneath the bore front, generated near the bed. These large vortical structures remained next to the bed as these persisting coherent structures were advected towards the left side of the numerical domain while the breaking bore propagated upstream, towards the right side of the numerical domain. The height of these large eddies was measured to reach up to approximately half of the downstream water depth, at the time of their generation. The whole sequence was detailed and commented. These original results confirmed and illustrated the experimental observations, identifying in particular coherent vortical recirculations under tidal bores.

However, the preliminary numerical works demonstrated the need for some more realistic turbulent inflow conditions to be specified at the inlet boundary. Some numerical simulations were tested by generating some turbulent inflow data consisting of the time-averaged experimental velocity profile with some superimposed random fluctuations. The generated data did not exhibit any spatial or temporal correlations, and the pseudo turbulence was quickly dissipated. Since turbulence is a three-dimensional physical feature, it was decided to investigate the three-dimensional numerical simulations of this phenomenon. The first numerical results are presented herein.

4.4. Three-Dimensional Numerical Simulation

An effective method to generate synthetic eddies on the inlet plane was implemented (JARRIN et al. 2006). The large eddy simulation (LES) of spatially developing flows such as open-channel flows requires the specification of instantaneous turbulent inlet fluctuations, which depends on the nature of the upstream flow. The synthetic eddy method (SEM) generates explicitly large scale coherent structures that are convected with the mean flow through the inlet plane (JARRIN et al. 2006). The method is based on the classic view of turbulence as a superposition of coherent structures. The method then generates a stochastic signal with prescribed mean velocity, Reynolds stresses, and length and time scale distributions. The number of eddies is a fixed parameter chosen before running the simulation. Although the SEM involves the summation of a large number of eddies for each grid point on the inflow, the CPU time required to generate the inflow data at each iteration is negligible (JARRIN et al. 2006).

The same experimental channel, presented in the previous section, was used: the test section was 12 m long and 0. 5 m wide, with smooth PVC bed and glass walls. Detailed velocity and free-surface elevation measurements were performed with an Acoustic Doppler Velocimeter (ADV) located at a distance x = 5 m from the channel intake, on the channel centreline (KOCH and CHANSON 2009). An acoustic displacement meter sampled the free-surface elevation immediately above the ADV sampling volume. Thus, to save CPU time, the 3D numerical domain was chosen to be 5 m long, using the experimental data to feed the inflow boundary condition calculated with the SEM method.

The 3D numerical domain was 5 m long, 1 m high and 0. 5 m wide. The initial water depth was d_1 = 0. 0785 m, and the same initial conditions and physical characteristics were identical to those used for the 2D simulations. The numerical domain was discretised into 500×500×20 regular Cartesian cells and it was partitioned into 512 sub-domains (one processor per sub-domain). The tidal bore Froude number was still Fr_1 = 1. 77.

KOCH and CHANSON (2005,2009) indicated that the tidal bores were sensitive to the turbulent characteristics of the inflow. The inlet velocity was calculated at the right side of the numerical domain at the inlet height $h_{in} = d_1$ = 0. 0785 m using the SEM method. KOCH and CHANSON (2005) showed that the initial flow was not fully-developed in the first half of the channel. At x = 5 m, the boundary layer thickness was estimated as δ/d_1 = 0. 6 to 0. 8. The velocity distribution and the free-stream velocity were given by KOCH and CHANSON (2005). NEZU (2005) proposed some pseudo-universal functions for the turbulence intensities v_x', v_y' and v_z'. These functions were successfully compared to the experimental data by KOCH and CHANSON (2005).

The 3D numerical simulation of the weak breaking bore generation and propagation first required some simulation time for the SEM turbulent boundary condition to propagate along the rectangular open-channel. Then, the wall boundary condition was set at the left side of the numerical domain to mimic the experimental closing gate. Figure 4-2 illustrates the generation and the propagation of the weak breaking tidal bore. Figure 4-3 shows some details of the tidal bore front at two different times. It can be seen that the complicated 3D interface deformations were well reproduced by the numerical simulation. For example, let us compare Figure 4-3 with Figure 3-3B. These preliminary results are in general accordance with the experimental observations concerning the free-surface deformations and the bore front propagation, and encouraging for further quantitative analysis.

Figure 4-2. Tidal bore generation and propagation at various times (3D modelling): $Fr_1 = 1.77$, $\rho \times (V_1+U) \times d_1/\mu = 1.2 \times 10^5$, $d_1 = 0.0785$ m, $V_1 = 1.02$ m/s, $B = 0.5$ m - The weak breaking tidal bore propagates from the left side to the right side of the numerical domain.

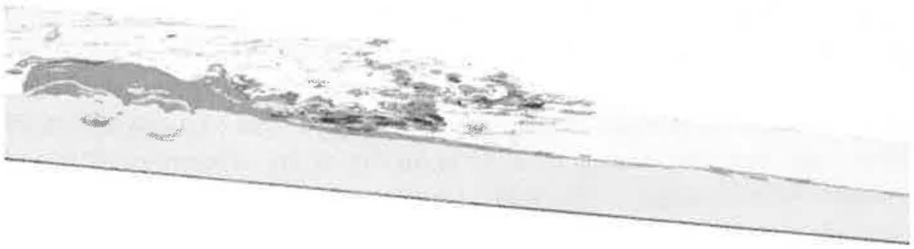

(A) t = 1. 85 s

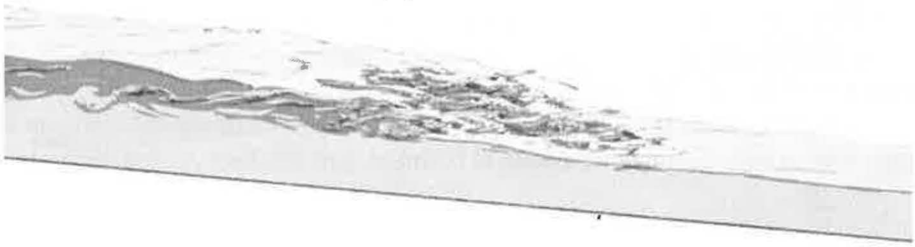

(B) t = 3. 62 s

Figure 4-3. Details of the tidal bore front (3D modelling) at t = 1. 85 s and 3. 62 s after gate closure: $Fr_1 = 1.77$, $\rho\times(V_1+U)\times d_1/\mu = 1.2\times10^5$, $d_1 = 0.0785$ m, $V_1 = 1.02$ m/s, B = 0. 5 m - Bore propagation from left to right.

5. UNSTEADY TURBULENCE PROPERTIES IN SURGES, BORES AND JUMPS

5.1. Presentation

In a turbulent tidal bore, a time-average is not a meaningful quantity because the hydrodynamic shock and the high-frequency turbulent fluctuations must be treated separately. A solution consists in repeating the experiments many times; the average of the instantaneous data (i. e. the ensemble-average) is the relevant mean property at a point at an instant. An experimental study reproduced 25 identical runs of a breaking tidal bore and the free-surface measurements were ensemble-averaged (DOCHERTY and CHANSON 2010). The experimental data are presented in Figure 5-1. Figure 5-1A presents the original data of the instantaneous water depth as a function of time. Figure 5-1B shows the ensemble-averaged median water depth d_{median} as a function of time, as well as the ensemble-averaged differences between 3rd and 4th quartiles (d_{75}-d_{25}) and 90% and 10% percentiles (d_{90}-d_{10}), and the maximum height between minimum and maximum water depth measurements (d_{max}-d_{min}).

Figure 5-1 illustrates that a single experiment cannot describe accurately the fluctuating nature of the tidal bore free-surface, but the ensemble-averaged data provides some useful information on the free-surface fluctuations. The free-surface measurements highlighted that that the free-surface fluctuations were the largest next to the roller toe and impingement point, and they decayed quasi-exponentially with increasing time as the bore roller passed beneath the sensor. The maximum free-surface fluctuations were observed during the first third of the bore roller passage. The trend was consistent with the findings of MOUAZE et al. (2005) and MURZYN and CHANSON (2009) in stationary hydraulic jumps.

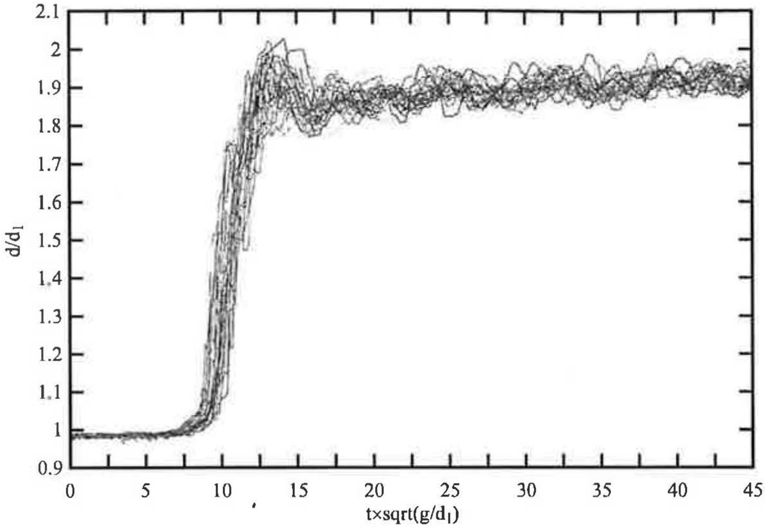

(A) Time-variations of the water depth in a breaking bore: superposition of 25 experimental repeats

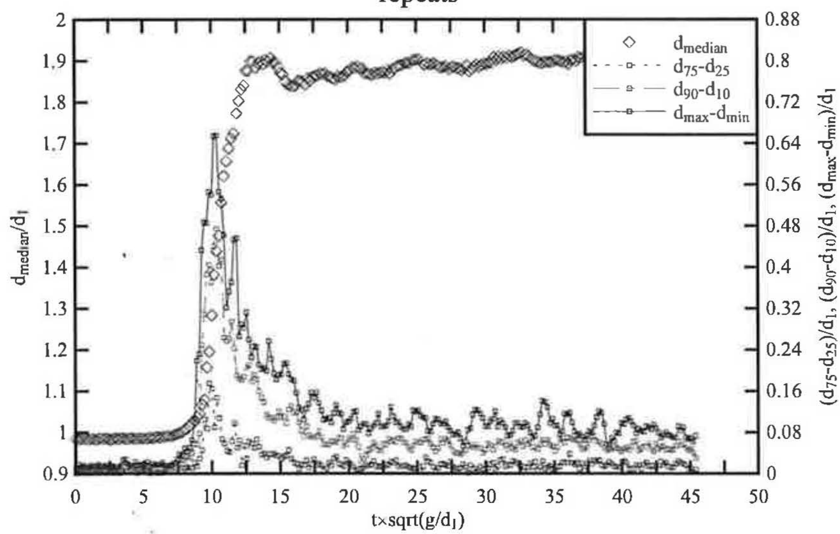

(B) Ensemble-average median water depth d_{median}, difference between 3rd and 4th quartiles $(d_{75}-d_{25})/d_1$ and 90% and 10% percentiles $(d_{90}-d_{10})/d_1$, and range of maximum to minimum water depth $(d_{max}-d_{min})/d_1$

Figure 5-1. Unsteady free-surface fluctuations in a breaking tidal bore – $d_1 = 0.119$ m, $Fr_1 = 1.65$, $\rho\times(V_1+U)\times d_1/\mu = 2.1\times10^5$, smooth PVC bed (Data: DOCHERTY and CHANSON 2010).

5.2. Unsteady Turbulence Properties

Both the ensemble-average method (EA) and the variable interval time average technique (VITA) were tested in a breaking tidal bore (DOCHERTY and CHANSON 2010). The ensemble-average technique was based upon the repetition of 20 identical experiments. Figure 5-2 presents the instantaneous water depth and longitudinal velocity for one experiment (Run 1). For the same flow conditions, Figure 5-2 shows the median water depth d_{median}, the ensemble-average (EA) median longitudinal velocity component V_{median} (median of 20 runs, thick red dashed line), the median value of VITA velocity (median value of 20 runs, thick blue dashed line), and all the VITA velocity for each of the 20 runs (thin black dotted line). Both the median VITA value for the 20 runs and EA median data yielded very close results in terms of both water depth and longitudinal velocity. The finding is interesting considering that the ensemble-averaging method required significantly less post-processing, and tended to suggest the sound selection of the threshold frequency F_{cutoff} for the VITA technique. However the VITA data based upon a single run highlighted some difference with the EA results (Figure 5-2B). The time-variations of the VITA data for each individual run presented some scatter compared to the ensemble-averaged median value (Figure 5-2B). Lastly note the scatter of the ensemble-averaged data around the long-term tend. It is acknowledged that the number of experimental repeats (20 herein) was small.

Figure 5-3 shows some comparison between some free-surface fluctuations (d_{75}-d_{25}) and some velocity fluctuations (V_{75}-V_{25}). The graphs present the median water depth d_{median} and the difference between 3rd and 4th quartiles for the water depth (d_{75}-d_{25}). Each graph includes further the median velocity component V_{median} (median of 20 runs) and the difference between 3rd and 4th quartiles (V_{75}-V_{25}), as well as the median value of the variable interval time average (VITA) velocity component (median value of 20 runs). Herein the median water depth and velocity components were ensemble-averaged over the 20 runs, and the median VITA value was calculated as the median VITA for the 20 Runs. The experimental results showed that the passage of the roller was always associated in some large free-surface fluctuations, associated with some large longitudinal velocity fluctuations and some upwards flow motion ($V_z > 0$) (Figure 5-3C & 5-3B). The effect of the sampling volume vertical elevation is illustrated in Figure 5-3 in terms of the horizontal and vertical velocity components. The transient recirculation region ("bubble") was restricted to the flow region next to the bed: $z/d_1 < 0.31$ for that experiment. In the upper flow region, no negative longitudinal velocity was recorded (Figure 5-3A & 5-3B).

For the same data set down in Figures 5-1 to 5-3, the instantaneous turbulent stresses were calculated using the ensemble-averaging (EA) and variable interval time averaging (VITA) techniques. Some typical results are presented in Figure 5-4. In Figure 5-4, the median Reynolds stress tensor components were calculated using either the ensemble-averaging (EA) and variable interval time averaging (VITA) methods (median value of 20 runs). The turbulent stress results showed a number of seminal features. Overall the turbulent stress data suggested that the passage of breaking tidal bores was associated with large turbulent stresses at all vertical elevations. That is, the magnitude of the Reynolds stress tensor components was significantly larger than prior to the bore passage. The finding was consistent with the observations of KOCH and CHANSON (2009), but that study deduced the turbulent stresses from a VITA analysis of a single experiment. KOCH and CHANSON did not present any ensemble-averaged nor VITA median data. Second, both the ensemble-averaging and variable interval time averaging techniques yielded comparable results (Figure 5-4).

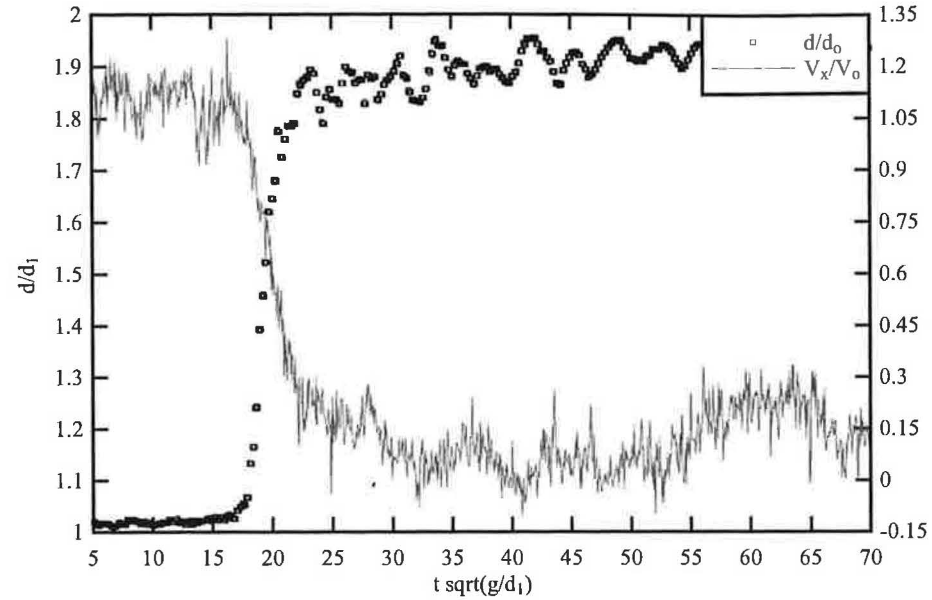

(A) Instantaneous water depth and longitudinal velocity (Run 1)

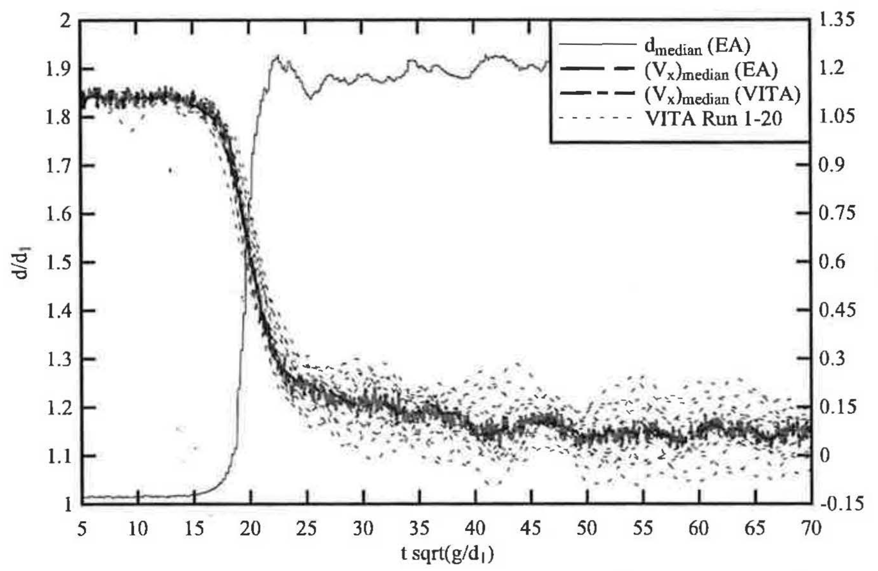

(B) Ensemble-average median water depth d_{median}, ensemble-average median velocity component V_{median}, median value of the variable interval time average (VITA) velocity component (median value of 20 runs), and low-pass filtered velocity components (VITA Runs 1 to 20) - VITA cutoff frequency: 2 Hz

Figure 5-2. Water depth and longitudinal velocity component in a breaking tidal bore - $d_1 = 0.117$ m, $Fr_1 = 1.61$, $\rho \times (V_1+U) \times d_1/\mu = 2.0 \times 10^5$, $z/d_1 = 0.434$, smooth PVC bed (Data: DOCHERTY and CHANSON 2010).

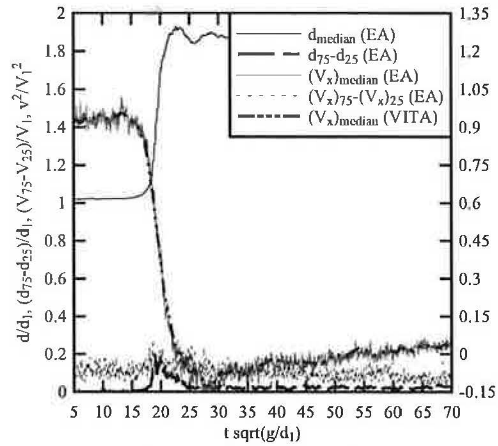

(A) Horizontal velocity, $z/d_1 = 0.135$

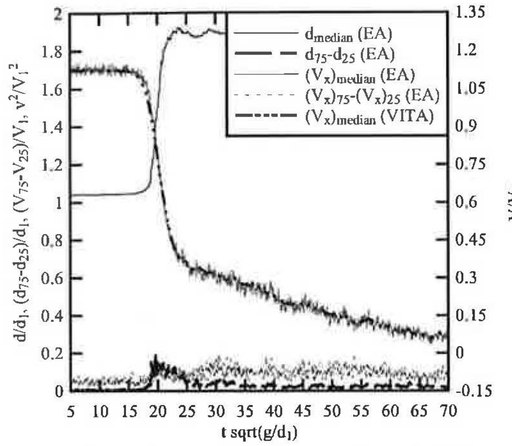

(B) Horizontal velocity, $z/d_1 = 0.733$

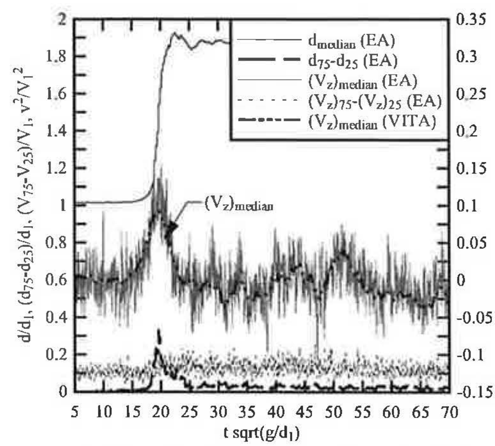

(C) Vertical velocity, $z/d_1 = 0.434$

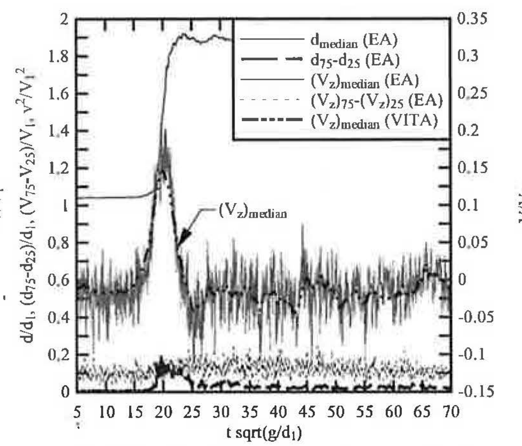

(D) Vertical velocity, $z/d_1 = 0.733$

Figure 5-3. Ensemble-average (EA) median water depth d_{median}, difference between 3rd and 4th quartiles of the water depth (d_{75}-d_{25}), ensemble-average median velocity component V_{median}, difference between 3rd and 4th quartiles of the velocity component (V_{75}-V_{25}), and median value of the variable interval time average (VITA) velocity component (median value of 20 runs) - $d_1 = 0.117$ m, $Fr_1 = 1.61$, $\rho\times(V_1+U)\times d_1/\mu = 2.0\times10^5$, $z/d_1 = 0.434$, smooth PVC bed (Data: DOCHERTY and CHANSON 2010) - VITA cutoff frequency: 2 Hz.

6. CONCLUSION

A tidal bore is an intriguing geophysical flow. It is a hydrodynamic shock characterised by a sudden rise in free-surface elevation associated with a discontinuity of the pressure and velocity fields. The propagation of tidal bores induces some substantial turbulent mixing in natural estuaries. A tidal bore is an unsteady turbulent flow, and this contribution focused on the unsteady turbulence of the process. Both physical and numerical modelling techniques were used in a complementary manner in absence of detailed field measurements.

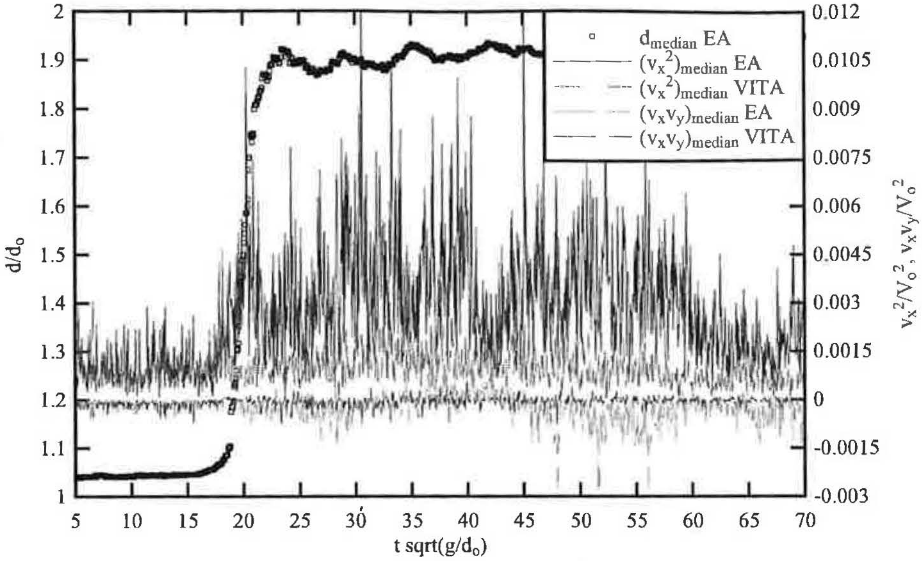

(A) Median Reynolds stresses v_x^2/V_o^2 and $v_x \times v_y/V_o^2$

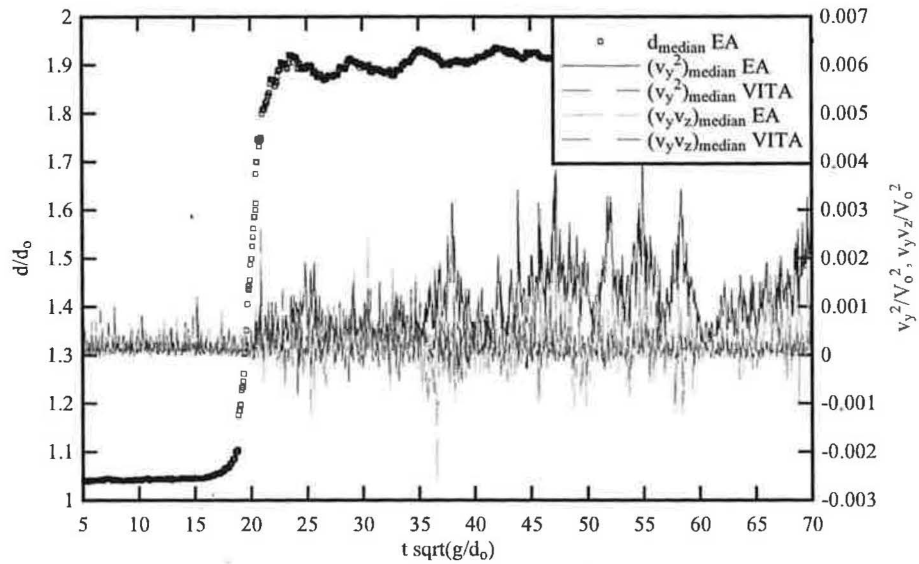

(B) Median Reynolds stresses v_y^2/V_o^2 and $v_y \times v_z/V_o^2$

Figure 5. 4. Ensemble-average median water depth d_{median}/d_o and median Reynolds stresses v_x^2/V_o^2 and $v_x \times v_y/V_o^2$, and v_y^2/V_o^2 and $v_y \times v_z/V_o^2$ in a breaking tidal bore - Comparison between ensemble-averaged and VITA calculations - d_1 = 0. 117 m, Fr_1 = 1. 61, $\rho \times (V_1+U) \times d_1/\mu = 2. 0 \times 10^5$, z/d_1 = 0. 733, smooth PVC bed (Data: DOCHERTY and CHANSON 2010).

An undular (non-breaking) bore is typically observed for a tidal bore Froude number less than 1. 5 to 1. 8. The wave front consists of a wave followed by a train of well-defined free-surface undulations called "whelps" in estuaries. For Froude numbers greater than 1. 5 to 1. 8, a breaking bore is observed with a marked roller, although some surface upward curvature ahead of the roller is observed. The instantaneous velocity measurements show a marked effect of the tidal bore front passage. The streamwise velocities are always characterised by a rapid flow deceleration at all vertical elevations, and large fluctuations of all velocity components are recorded beneath the surge and whelps. A comparison between undular and breaking surge data suggest some basic difference. In a breaking surge, some large turbulent stresses are observed next to the shear zone in a region of high velocity gradients. Next to the bed, however, some transient flow recirculation is observed. In an undular bore, some large velocity fluctuations and Reynolds stresses are recorded beneath the first wave crest and the secondary waves (free-surface undulations), implying a long-lasting effects after the bore front passage.

Both physical and numerical studies documented the production of large coherent structures in tidal bores. The existence of such energetic turbulent events beneath and shortly after the tidal bore front implied the generation of vorticity during the bore propagation. The presence of these persisting coherent structures indicated that a great amount of sediment materials could be placed into suspension and transported by the main flow in a natural system. Overall the experimental findings are consistent with field observations and anecdotal evidences. These show in particular the significant impact of tidal bores on natural channels and their eco-systems.

A comparison between ensemble-average (EA) and variable interval time average (VITA) velocity data is presented for a tidal bore experiment. Both the EA and VITA results show some comparable velocity pattern with some relatively-long-term data trend superposed to some high-frequency turbulent fluctuations. While both methods should converge to the same asymptotic trend, the data show that the VITA calculations over a single experiment present some non-negligible difference with the EA median value for all velocity components. The EA median value and the median of 20 VITA yield very close results suggesting a sound selection of cutoff frequency. The turbulent stress data highlight some larger median Reynolds stresses during and shortly after the tidal bore passage than prior to.

Overall the study demonstrates the intensive turbulence and turbulent mixing generated by a tidal bore, together with the complicated features of the unsteady turbulent structures. Simply a tidal bore remains a challenging research topic to theoreticians, numericians and experimentalists.

ACKNOWLEDGMENTS

The first author acknowledges the experimental works of his students Dr Christian KOCH and Nicholas J. DOCHERTY. The authors thank the Aquitaine Regional Council for the financial support dedicated to a 256-processor cluster investment, located in the TREFLE laboratory. This study was granted access to the HPC resources of CINES under the allocation 2009-c2009026104 made by Grand Equipement National de Calcul Intensif (GENCI). The authors thank Dr Hubert BRANGER for his detailed and valuable input.

NOTATION

A	flow cross-section area (m^2);
B	channel width (m);

C	phase function, or liquid fraction, defined as: C = 0 in air and C = 1 in water;
d	(a) flow depth (m) measured normal to the invert;
	(b) flow depth (m) measured above the fixed bed roughness;
d_1	initial flow depth (m) measured normal to the chute invert;
d_2	conjugate flow depth (m) measured immediately behind the tidal bore front;
F	frequency (Hz);
F_{cutoff}	cutoff frequency (Hz) for low/high pass filtering;
Fr_1	tidal bore Froude number defined as: $Fr_1 = (V_1 + U)/\sqrt{g \times d_1}$;
g	gravity constant (m/s^2): g = 9. 80 m/s^2 in Brisbane, Australia;
k_s	equivalent sand roughness height (m);
L	length (m);
L_r	geometric scaling ration defined at the ratio of prototype to model dimensions;
N	(a) number of samples;
	(b) number of experimental repeats;
P	pressure (Pa);
p	pressure fluctuation (Pa);
Q	volume flow rate (m^3/s);
q	volume flow rate per unit width (m^2/s): q = Q/B;
Re	Reynolds number: for a tidal bore $Re = \rho \times (V_1 + U) \times d_1 / \mu$;
R_{ij}	normalised cross-correlation coefficient;
R_{ijk}	normalised triple correlation coefficient;
S_o	bed slope: $S_o = \sin\theta$;
T	averaging period (s);
t	time (s);
t'	time (s);
U	tidal bore front celerity (m/s) for an observer standing on the bank, positive upstream;
V	(a) flow velocity (m/s) positive downstream;
	(b) instantaneous velocity component (m/s);
V_1	initial flow velocity (m/s) positive downstream: $V_1 = q/d_1$;
V_2	conjugate flow velocity (m/s) positive downstream;
V_x	longitudinal velocity (m/s) positive downstream;
V_y	transverse velocity (m/s) positive towards the left sidewall;
V_z	vertical velocity (m/s) positive upwards;
$\overline{V}$	(a) time-averaged velocity (m/s);
	(b) ensemble-averaged (EA) velocity (m/s);
	(c) variable interval time averaged (VITA) velocity (m/s);
v	turbulent velocity fluctuation (m/s): $v = V - \overline{V}$;
v'	root mean square of turbulent velocity component (m/s);
x	longitudinal distance (m) measured from the channel upstream end, positive downstream;
y	transverse distance (m) measured from the channel centreline, positive towards the left sidewall;

z	distance (m) normal to the bed; it is the vertical distance (m) for a horizontal channel; for the fixed rough bed, z is measured above the top of the bed roughness;

Greek Symbols

δ	boundary layer thickness (m) defined in terms of 99% of the free-stream velocity;
μ	dynamic viscosity (Pa. s);
μ_T	turbulent viscosity (Pa. s);
π	π = 3. 141592653589793238462643;
θ	bed slope angle with the horizontal, positive downwards;
ρ	density (kg/m^3);
σ	surface tension (N/m);

Subscript

a	air;
max	maximum value;
median	median value (i. e. 50% percentile);
min	minimum value;
w	water;
x	longitudinal component positive downstream;
y	component transverse to the channel centreline;
z	component normal to the invert;
1	initial flow conditions: i. e., upstream of the tidal bore front;
2	conjugate flow conditions: immediately after the tidal bore passage;
10	10% percentile;
25	25% percentile;
75	75% percentile;
90	90% percentile;

Abbreviations

ADV	acoustic Doppler velocimetry;
BICGStab	bi-conjugate gradient stable algorithm;
EA	ensemble average;
GMRES	generalised minimal residual method;
HYPRE	high performance preconditionners;
LDA	laser Doppler anemometry;
MPI	message passing interface;
PIV	particle image velocimetry;
VITA	variable interval time average;

Notation

Ø	diameter;
$\frac{\partial}{\partial y}$	partial differentiation with respect to y.

REFERENCES

Barnes, M. P., O'donoghue, T., Alsina, J. M. & Baldock, T. E. (2009). "Direct Bed Shear Stress Measurements in Bore-Driven Swash." *Coastal Eng.,* Vol. *56,* No. 8, 853-867.

Bellal, M., Spinewine, B., Savary, C. & Zech, Y. (2003). "Morphological Evolution of Steep-Sloped River Beds in the Presence of a Hydraulic Jump: Experimental Study." *Proc. 30th IAHR Biennial Congress*, Thessaloniki, Greece, Theme C, Vol. *II,* 133-140.

Benet, F. & Cunge, J. A. (1971). "Analysis of Experiments on Secondary Undulations caused by Surge Waves in Trapezoidal Channels." *Jl of Hyd. Res.,* IAHR, Vol. *9,* No. 1, 11-33.

Benjamin, T. B. & Lighthill, M. J. (1954). "On Cnoidal Waves and Bores." *Proc. Royal Soc. of London, Series A, Math. & Phys. Sc.,* Vol. *224,* No. 1159, 448-460.

Bradshaw, P. (1971). "An Introduction to Turbulence and its Measurement." Pergamon Press, Oxford, UK, *The Commonwealth and International Library of Science and technology Engineering and Liberal Studies*, Thermodynamics and Fluid Mechanics Division, 218 pages.

Bradshaw, P. (1976). "Turbulence." Springer-Verlag, *Topics in Applied Physics*, Vol. *12*, Berlin, Germany, 335 pages.

Butt, T., Russel, P., Puleo, J., Miles, J. & Masselink, G. (2004). "The Influence of Bore Turbulence on Sediment Transport in the Swash and Inner Surf Zones." *Cont. Shelf Res.,* Vol. *24,* 757-771.

Carling, P. A. (1995). "Flow-Separation Berms Downstream of a Hydraulic Jump in a Bedrock Channel." *Geomorphology*, Vol. *11,* 245-253.

Chanson, H. (1999). *"The Hydraulics of Open Channel Flow: An Introduction."* Edward Arnold, London, UK, 512 pages.

Chanson, H. (2000). "Boundary Shear Stress Measurements in Undular Flows : Application to Standing Wave Bed Forms." *Water Res. Res.,* Vol. *36,* No. 10, 3063-3076.

Chanson, H. (2004). *"The Hydraulics of Open Channel Flow: An Introduction."* Butterworth-Heinemann, 2nd edition, Oxford, UK, 630 pages.

Chanson, H. (2009a). "Current Knowledge In Hydraulic Jumps And Related Phenomena. A Survey of Experimental Results." *European Journal of Mechanics B/Fluids*, Vol. *28,* No. 2, 191-210 (DOI: 10. 1016/j. euromechflu. 2008. 06. 004).

Chanson, H. (2009b). "Applied Hydrodynamics: An Introduction to Ideal and Real Fluid Flows." *CRC Press*, Taylor & Francis Group, Leiden, *The Netherlands, 478* pages.

Chanson, H. (2010). "Unsteady Turbulence in Tidal Bores: Effects of Bed Roughness." *Journal of Waterway, Port, Coastal, and Ocean Engineering*, ASCE, Vol. 136, No. 5, pp. 247-256 (DOI: 10.1061/(ASCE)WW.1943-5460.0000048)

Chanson, H. (2010a). "Current Knowledge in Tidal bores and their Environmental, Ecological and Cultural Impacts." *Environmental Fluid Mechanics*, Vol. *10*, No. 4 (DOI: 10. 1007/s10652-009-9160-5). In print.

Chanson, H. (2010b). "Unsteady Turbulence in Tidal Bores: the Effects of Bed Roughness." *Journal of Waterway, Port, Coastal, and Ocean Engineering*, ASCE, Vol. *136* (DOI: 10. 1061/(ASCE)WW. 1943-5460. 0000048). In print.

Chanson, H. (2010c). "Turbulent Shear Stresses in Hydraulic Jumps and Decelerating Surges: An Experimental Study." *Earth Surface Processes and Landforms*, Vol. 35, incl. 2 video files In print.

CHEN, Jiyu, LIU, Cangzi, ZHANG, Chongle, & WALKER, H. J. (1990). "Geomorphological Development and Sedimentation in Qiantang Estuary and Hangzhou Bay." *Jl of Coastal Research*, Vol. *6*, No. 3, 559-572.

Cunge, J. A. (2003). "Undular Bores and Secondary Waves - Experiments and Hybrid Finite-Volume Modelling." *Jl of Hyd. Res.*, IAHR, Vol. *41*, No. 5, 557-558.

Docherty, N. J. & Chanson, H. (2010). "Characterisation of Unsteady Turbulence in Breaking Tidal Bores including the Effects of Bed Roughness." *Hydraulic Model Report No. CH76/10*, School of Civil Engineering, The University of Queensland, Brisbane, Australia, 106 pages.

Falgout, R. D., Jones, J. E. & Yang, U. M. (2006). "The Design and Implementation of Hypre, a Library of Parallel High Performance Preconditioners." in *"Numerical Solution of Partial Differential Equations on Parallel Computers"*, Springer-Verlag, Chap. 51, 267-294.

Favre, H. (1935). "Etude Théorique et Expérimentale des Ondes de Translation dans les Canaux Découverts." (*'Theoretical and Experimental Study of Travelling Surges in Open Channels.'*) Dunod, Paris, France (in French).

Furuyama, S. & Chanson, H. (2008). "A Numerical Study of Open Channel Flow Hydrodynamics and Turbulence of the Tidal Bore and Dam-Break Flows." *Hydraulic Model Report No. CH66/08*, Div. of Civil Engineering, The University of Queensland, Brisbane, Australia, May, 88 pages.

Garcia, C. M. & Garcia, M. H. (2006). "Characterization of Flow Turbulence in Large-Scale Bubble-Plume Experiments." *Experiments in Fluids*, Vol. *41*, No. 1, 91-101. .

Goda, K. (1978). "A Multistep Technique with Implicit Difference Schemes for Calculating Two- or Three-Dimensional Cavity Flows." *Jl. Comput. Phys.*, Vol. *30*, 76-95.

Grant, G. E. (1997). "Critical Flow Constrains Flow Hydraulics in Mobile-Bed Streams: a New Hypothesis." *Water Res. Res.*, Vol. 33, No. 2, 349-358. Discussion: Vol. *35*, No. 3, 903-908.

Henderson, F. M. (1966). "*Open Channel Flow.*" MacMillan Company, New York, USA.

Hinze, J. O. (1975). "*Turbulence.*" McGraw-Hill Publ., 2nd Edition, New York, USA.

Hornung, H. G., Willert, C. & Turner, S. (1995). "The Flow Field Downstream of a Hydraulic Jump." *Jl of Fluid Mech.*, Vol. *287*, 299-316.

Jarrin, N., Benhamadouche, S., Laurence, D. & Prosser, R. (2006). "A Synthetic Eddy-Method for Generating Inflow Conditions for Large-Eddy Simulations." *Int. Jl. Heat Fluid Flow*, Vol. *27*, 585-593.

Kennedy, J. F. (1963). "The Mechanics of Dunes and Antidunes in Erodible-Bed Channels." *Jl of Fluid Mech.*, Vol. *16*, No. 4, 521-544 (& 2 plates).

Kobayashi, N. (2001). "Sand Suspension, Storage, Advection, and Settling in Surf and Swash Zones." *Jl of Geophys. Res. -Oceans*, AGU, Vol. *106*, No. C5, 9363-9376.

Koch, C. & Chanson, H. (2005). "An Experimental Study of Tidal Bores and Positive Surges: Hydrodynamics and Turbulence of the Bore Front." *Report No. CH56/05*, Dept. of Civil Engineering, The University of Queensland, Brisbane, Australia, July, 170 pages.

Koch, C. & Chanson, H. (2008). "Turbulent Mixing beneath an Undular Bore Front." *Journal of Coastal Research*, Vol. *24*, No. 4, 999-1007 (DOI: 10. 2112/06-0688. 1).

Koch, C. & Chanson, H. (2009). "Turbulence Measurements in Positive Surges and Bores." *Journal of Hydraulic Research*, *IAHR*, Vol. *47*, No. 1, 29-40 (DOI: 10. 3826/jhr. 2009. 2954).

Leveque, R. J. (1992). "Numerical Methods for Conservation Laws." *Lectures in Mathematics*, Birkhauser, Zurich.

Liggett, J. A. (1994). *"Fluid Mechanics."* McGraw-Hill, New York, USA.

Lighthill, J. (1978). *"Waves in Fluids."* Cambridge University Press, Cambridge, UK, 504 pages.

Lubin, P., Glockner, S. & Chanson, H. (2010a). "Numerical Simulation of a Weak Breaking Tidal Bore." *Mechanics Research Communications*, Vol. *37*, No. 1, 119-121 (DOI: 10. 1016/j. mechrescom. 2009. 09. 008).

Lubin, P., Chanson, H. & Glockner, S. (2010b). "Large Eddy Simulation of Turbulence Generated by a Weak Breaking Tidal Bore." *Environmental Fluid Mechanics*, Vol. *10*, No. 4 (DOI: 10. 1007/s10652-009-9165-0). In print.

Macdonald, R. G., Alexander, J., Bacon, J. C. & Cooker, M. J. (2009). "Flow Patterns, Sedimentation and Deposit Architecture under a Hydraulic Jump on a Non-Eroding Bed: Defining Hydraulic Jump Unit Bars." *Sedimentology*, Vol. *56*, 1346-1367 (DOI: 10. 1111/j. 1365-3091. 2008. 01037. x).

Madsen, P. A., Simonsen, H. J. & Pan, C. -H. (2005). "Numerical Simulation of Tidal Bores and Hydraulic Jumps." *Coastal Engineering*, Vol. *52*, 409-433.

Mouaze, D., Murzyn, F. & Chaplin, J. R. (2005). "Free Surface Length Scale Estimation in Hydraulic Jumps." *Jl of Fluids Eng., Trans. ASME*, Vol. *127*, 1191-1193.

Murzyn, F. & Chanson, H. (2009). "Free-Surface Fluctuations in Hydraulic Jumps: Experimental Observations." *Experimental Thermal and Fluid Science*, Vol. *33*, No. 7, 1055-1064 (DOI: 10. 1016/j. expthermflusci. 06. 003).

Nezu, I. (2005). "Open-Channel Flow Turbulence and its Research prospect in the 21st Century." *Jl of Hyd. Engrg.*, ASCE, Vol. *131*, No. 4, 229-246.

Parker, G. (1996). "Some speculations on the relation between Channel Morphology and Channel Scale Flow Structures." in "*Coherent Flow structures in Open Channels*", John Wiley, Chichester, UK, P. J. ASHWORTH, S. J. BENNETT, J. L. BEST And S. J. Mclelland Ed., 423-458.

Parker, G. & Izumi, N. (2000). "Purely Erosional Cyclic and Solitary Steps Created by Flow over a Cohesive Bed." *Jl of Fluid Mech.*, Vol. *419*, 203-238.

Patankar, S. V. (1990). "*Numerical Heat Transfer and Fluid Flow.*" Hemisphere Publishing Corporation, New York, USA.

Piquet, J. (1999). "*Turbulent Flows. Models and Physics.*" Springer, Berlin, Germany, 761 pages.

Rayleigh, Lord (1908). "Note on Tidal Bores." *Proc. Royal Soc. of London, Series A containing Papers of a Mathematical and Physical Character*, Vol. *81*, No. 541, 448-449.

Reynolds, O. (1883). "An Experimental Investigation of the Circumstances which Determine whether the Motion of Water shall be Direct or Sinuous, and the Laws of Resistance in Parallel Channels." *Phil. Trans. Roy. Soc. Lond.*, Vol. *174*, 935-982.

Rouse, H. (1938). "*Fluid Mechanics for Hydraulic Engineers*." McGraw-Hill Publ., New York, USA (also Dover Publ., New York, USA, 1961, 422 pages)

Rudman, M. (1998). "A Volume-Tracking Method for Incompressible Multifluid Flows with Large Density Variations." *Int. Jl. Numer. Meth. Fluids*, Vol. *28*, No. 2, 357-378.

Sagaut, P. (1998). *"Large Eddy Simulation for Incompressible Flows - An Introduction."* Springer Verlag, Heidelberg, Germany.

Treske, A. (1994). "Undular Bores (Favre-Waves) in Open Channels - Experimental Studies." *Jl of Hyd. Res.*, IAHR, Vol. 32, No. 3, 355-370. Discussion : Vol. *33*, No. 3, 274-278.

Tull, K. A. (1997). "Spawning Activity of triped Bass in a Tidal Bore River: the Shubenacadie-Stewiacke System, Nova Scotia." *M. Sc. thesis*, University of East Carolina, Dept of Biology, 140 pages.

Wolanski, E., Williams, D., Spagnol, S. & Chanson, H. (2004). "Undular Tidal Bore Dynamics in the Daly Estuary, Northern Australia." *Estuarine, Coastal and Shelf Science*, Vol. *60*, No. 4, 629-636.

Yokokawa, M., Okuno, K., Nakamura, A., Muto, T., Miata, Y., Naruse, H. & Parker, G. (2009). "Aggradational Cyclic Steps: Sedimentary Structures Found in Flume Experiments." *Proc. 33rd IAHR Biennial Congress*, Vancouver, Canada, 5547-5554.

Internet References

Tidal bores, Mascaret, Pororoca . Myths, Fables and Reality !!!	{http://www. uq. edu. au/~e2hchans/tid_bore. html}
The Tidal Bore of the Seine River, France	{http://www. uq. edu. au/~e2hchans/mascaret. html}
Free-surface undulations in open channel flows: Undular jumps, Undular bores, Standing waves	{http://www. uq. edu. au/~e2hchans/undular. html}
Research publications by Hubert CHANSON	{http://espace. library. uq. edu. au/list/author_id/193/} at UQeSpace
UQeSpace open access repository	{http://espace. library. uq. edu. au/}
OAIster open acces catalogue	{http://www. oaister. org/}

Reviewed by Dr Hubert BRANGER, IRPHE/Luminy (France).

PHYSICS RESEARCH AND TECHNOLOGY

TURBULENCE

THEORY, TYPES AND SIMULATION

RUSSELL J. MARCUSO
EDITOR

NOVA

Nova Science Publishers, Inc.
New York